

Synthesis, NMR studies, and molecular orbital calculations on cyclohexadienyl derivatives of (η^6 -arene)tris(pyrazolyl)ruthenium(II) compounds

Sameer Bhambri,^a Andrea Bishop,^b Nikolas Kaltsoyannis^{*b} and Derek A. Tocher^{*a}

^a Department of Chemistry, University College London, 20 Gordon Street, London, UK WC1H 0AJ. E-mail: d.a.tocher@ucl.ac.uk

^b Centre for Theoretical and Computational Chemistry, University College London, 20 Gordon Street, London, UK WC1H 0AJ. E-mail: n.kaltsoyannis@ucl.ac.uk

Received 5th June 1998, Accepted 4th September 1998

The addition of nucleophiles to the complex cations $[\text{Ru}(\eta^6\text{-arene})\{\kappa^3\text{-HB}(\text{Pz}_3)\}]^+$ or $[\text{Ru}(\eta^6\text{-arene})\{\kappa^3\text{-HC}(\text{Pz}_3)\}]^{2+}$ (Pz = pyrazol-1-yl) proceeds smoothly to give $[\text{Ru}(\eta^5\text{-cyclohexadienyl})\{\kappa^3\text{-HB}(\text{Pz}_3)\}]$ or $[\text{Ru}(\eta^5\text{-cyclohexadienyl})\{\kappa^3\text{-HC}(\text{Pz}_3)\}]^+$ respectively, which have been identified by NMR spectroscopy. NMR spectroscopy reveals that each of the cyclohexadienyl derivatives exhibits significant barriers to rotation of the η^5 ligand. The electronic structure of $[\text{Ru}(\eta^6\text{-arene})\{\kappa^3\text{-HB}(\text{Pz}_3)\}]^+$ and the cyclohexadienyl derivatives has been probed by extended Hückel molecular orbital calculations, with emphasis on the rationalisation of the experimentally observed barriers to rotation of the carbocycles. The single crystal structure of $[\text{Ru}(\eta^5\text{-C}_6\text{H}_6\text{CN})\{\kappa^3\text{-HC}(\text{Pz}_3)\}][\text{PF}_6]$ is reported.

Introduction

In the past we have examined the attack of hydride and other nucleophiles on the arenes in a range of $[\text{Ru}(\eta^6\text{-arene})(\eta^6\text{-[2.2]paracyclophane})]^{2+}$ complexes.^{1,2} These reactions can be used for the synthesis of a number of cyclohexadienyl³⁻⁷ and diene^{8,9} derivatives. However, the nature of the products is highly dependent upon the details of the synthetic procedure, and changes in solvent, the hydridic reagent, and the method of work-up can radically affect the identity of the isolated products.² While the properties of the [2.2]paracyclophane ligand are such that in the case of double nucleophilic attack we can guarantee that diene containing complexes are formed in preference to bis(cyclohexadienyl) containing ones we nevertheless have little control over whether the new complex contains a 1,3- or 1,4-diene. Indeed in many instances a mixture of both is present in the isolated product. While this is an interesting observation it does limit the practical application of this chemistry from the point of view of arene and diene functionalisation. As a consequence of this we set out to develop a range of compounds in which the spectator ligand could exert some steric control on the chemistry occurring at the coordinated arene. The complexes which we have focused on are a selection of $[\text{Ru}(\eta^6\text{-arene})\{\kappa^3\text{-HB}(\text{Pz}_3)\}]^+$ and $[\text{Ru}(\eta^6\text{-arene})\{\kappa^3\text{-HC}(\text{Pz}_3)\}]^{2+}$ (Pz = pyrazol-1-yl) derivatives in which one might imagine that substituents in the '3' position on the pyrazolyl rings would interact with the π -bound arene to influence its reactivity.^{10,11} Preliminary results¹² indicated that while the interaction with the coordinated arene might be limited there is evidence of significant interaction in the cyclohexadienyl products formed by the attack of a single nucleophile. That interaction has now been extensively explored, is clearly a function of the substituents on the carbocyclic ring, and is the focus of this report.

Experimental and computational details

Instrumental

Infrared spectra were recorded on a Nicolet-205 spectrometer between 4000 and 400 cm^{-1} as KBr discs. NMR spectra were

recorded on Varian VXR400 or Bruker 300 spectrometers and referenced internally against the residual protons of the deuterated solvents (d^6 -DMSO, d^6 -acetone, CDCl_3 , and CD_2Cl_2). Microanalyses were carried out by the departmental service at University College London. Fast atom bombardment mass spectra (assignments based on the ¹⁰²Ru isotope) were recorded by the University of London Intercollegiate Research Service (ULIRS) at the London School of Pharmacy. All manipulations were carried out under nitrogen with degassed laboratory grade solvents using conventional Schlenk-line techniques.

Starting materials

Ruthenium trichloride hydrate was obtained on loan from Johnson Matthey plc and was purified before use by repeated dissolution in water and boiling to dryness. The compounds $[\text{Ru}(\eta^6\text{-arene})\{\kappa^3\text{-HB}(\text{Pz}_3)\}][\text{PF}_6]$, $[\text{Ru}(\eta^6\text{-C}_6\text{H}_6)\{\kappa^3\text{-HB}(3,5\text{-Me}_2\text{Pz}_3)\}][\text{PF}_6]$, and $[\text{Ru}(\eta^6\text{-arene})\{\kappa^3\text{-HC}(\text{Pz}_3)\}][\text{PF}_6]_2$ were synthesised as reported previously.^{10,11}

Preparations

$[\text{Ru}(\eta^5\text{-C}_6\text{H}_7)\{\kappa^3\text{-HB}(\text{Pz}_3)\}]$ 1. $[\text{Ru}(\eta^6\text{-C}_6\text{H}_6)\{\kappa^3\text{-HB}(\text{Pz}_3)\}][\text{PF}_6]$ (0.09 g, 0.16 mmol) was suspended in degassed thf (10 cm^3) and treated with $\text{Na}[\text{BH}_4]$ (0.05 g, excess). After stirring for 1 h at room temperature the solution was filtered through Celite to remove any unreacted $\text{Na}[\text{BH}_4]$. Evaporation of the resulting filtrate to dryness gave **1** as a pale yellow air sensitive residue. Yield: 0.05 g, 0.12 mmol, 75% (Found: C, 45.5; H, 4.5; N, 21.4. Calc. for $\text{C}_{15}\text{H}_{17}\text{N}_6\text{BRu}$: C, 45.9; H, 4.4; N, 21.4%). Mass spectrum: m/z 393 $[\text{M} - \text{H}]^+$. Infrared: $\nu(\text{BH})$ 2494, $\nu(\text{CH}_{\text{endo}})$ 2963, $\nu(\text{CH}_{\text{exo}})$, 2782 cm^{-1} .

$[\text{Ru}(\eta^5\text{-C}_6\text{H}_6\text{CN})\{\kappa^3\text{-HB}(\text{Pz}_3)\}]$ 2. $[\text{Ru}(\eta^6\text{-C}_6\text{H}_6)\{\kappa^3\text{-HB}(\text{Pz}_3)\}][\text{PF}_6]$ (0.05 g, 0.09 mmol) was suspended in degassed thf and treated with KCN (0.05 g, excess). The mixture was stirred at room temperature for 2 h and then pumped to dryness. Extraction into chloroform followed by filtering through Celite and evaporation to dryness gave **2** as an air stable yellow residue. Yield: 0.033 g, 0.079 mmol, 84% (Found: C, 46.1; H,

3.8; N, 23.3. Calc. for $C_{16}H_{16}N_7BRu$: C, 45.9; H, 3.9; N, 23.5%. Mass spectrum: m/z 419 $[M]^+$, 393 $[M - CN]^+$. Infrared: $\nu(BH)$ 2484, $\nu(CN)$ 2214, $\nu(CH_{endo})$ 2945 cm^{-1} .

[Ru(η^5 -C₆H₆OH){κ³-HB(Pz)₃}] 3. [Ru(η^6 -C₆H₆){κ³-HB(Pz)₃}] $[PF_6]$ (0.050 g, 0.09 mmol) was suspended in degassed methanol (10 cm³) and treated with methanolic KOH (0.047 g, excess). The mixture was stirred at room temperature for 48 h and then evaporated to dryness. Extraction into thf followed by filtration through Celite and evaporation to dryness gave **3** as a yellow powder. Yield: 0.031 g, 0.08 mmol, 81% (Found: C, 43.7; H, 4.1; N, 20.1. Calc. for $C_{15}H_{17}N_6BORu$: C, 44.0; H, 4.2; N, 20.5%). Mass spectrum: m/z 393 $[M - OH]^+$. Infrared: $\nu(BH)$ 2497, $\nu(OH)$ 3450, $\nu(CH_{endo})$ 2950 cm^{-1} .

[Ru(η^5 -C₆H₆D){κ³-HB(Pz)₃}] 4. [Ru(η^6 -C₆H₆){κ³-HB(Pz)₃}] $[PF_6]$ (0.08 g, 0.16 mmol) was treated with Na[BD₄] (0.04 g, excess) and worked up as described for **1**. Yield: 0.05 g, 0.12 mmol, 77%. Mass spectrum: m/z 393 $[M - D]^+$. Infrared: $\nu(BH)$ 2492, $\nu(CH_{endo})$ 2933, $\nu(CD_{exo})$ 2088 cm^{-1} .

[Ru(η^5 -1-ⁱPr-4-MeC₆H₃){κ³-HB(Pz)₃}] 5a and 5b. [Ru(η^6 -1-ⁱPr-4-MeC₆H₄){κ³-HB(Pz)₃}] $[PF_6]$ (0.124 g, 0.21 mmol) was suspended in degassed thf (10 cm³) and treated with Na[BH₄] (0.05 g, excess). After stirring for 2 h at room temperature the solution was filtered through Celite to remove any unreacted Na[BH₄]. Evaporation of the resulting filtrate to dryness led to deposition of a crude yellow product. Purification by passing a diethyl ether solution of **5** down an alumina column (mesh 100–250) with subsequent evaporation to dryness of the eluent resulted in isolation of **5a** and **5b** as a mildly air sensitive solid. The two isomers were not separated. Yield: 0.076 g, 0.17 mmol, 82% (Found: C, 50.8; H, 5.5; N, 18.5. Calc. for $C_{19}H_{25}N_6BRu$: C, 50.8; H, 5.6; N, 18.7%). Mass spectrum: m/z 450 $[M]^+$. Infrared: $\nu(BH)$ 2452, $\nu(CH_{endo})$ 2922, $\nu(CH_{exo})$ 2776 cm^{-1} .

[Ru(η^5 -1-ⁱPr-4-MeC₆H₄CN){κ³-HB(Pz)₃}] 6a and 6b. [Ru(η^6 -1-ⁱPr-4-MeC₆H₄){κ³-HB(Pz)₃}] $[PF_6]$ (0.134 g, 0.23 mmol) was suspended in degassed thf (15 cm³) and treated with KCN (0.05 g, excess). The mixture was refluxed for 5 d then filtered and evaporated to dryness. Purification was carried out by repeated extraction of the residue with CHCl₃. The two isomers of **6** were not separated. Yield: 0.067 g, 0.14 mmol, 63%. (Found: C, 49.6; H, 5.2; N, 20.8. Calc. for $C_{20}H_{24}N_7BRu$: C, 50.0; H, 5.1; N, 20.7%). Mass spectrum: m/z 449 $[M - CN]^+$. Infrared: $\nu(BH)$ 2456, $\nu(CH_{endo})$ 2931, $\nu(CN)$ 2221 cm^{-1} .

[Ru(η^5 -1-ⁱPr-4-MeC₆H₄OH){κ³-HB(Pz)₃}] 7a and 7b. [Ru(η^6 -1-ⁱPr-4-MeC₆H₄){κ³-HB(Pz)₃}] $[PF_6]$ (0.110 g, 0.19 mmol) was suspended in degassed thf (15 cm³) and treated with NaOH (0.05 g, excess). The mixture was refluxed for 4 d then filtered and evaporated to dryness. The purification procedure was similar to that for **5**. The isomers of **7** were not separated. Yield: 0.053 g, 0.11 mmol, 61% (Found: C, 49.9; H, 5.3; N, 18.0. Calc. for $C_{19}H_{25}N_6BORu$: C, 49.1; H, 5.4; N, 18.1%). Mass spectrum: m/z 449 $[M - OH]^+$. Infrared: $\nu(BH)$ 2460, $\nu(CH_{endo})$ 2959, $\nu(OH)$ ca. 3400 cm^{-1} .

[Ru(η^5 -1,4-Me₂C₆H₃){κ³-HB(Pz)₃}] 8. [Ru(η^6 -1,4-Me₂C₆H₄){κ³-HB(Pz)₃}] $[PF_6]$ (0.121 g, 0.23 mmol) was suspended in degassed thf (15 cm³) and treated with Na[BH₄] (0.05 g, excess). The mixture was refluxed for 2 h then filtered and evaporated to dryness. The crude residue was extracted with chloroform, filtered through Celite and evaporated to dryness to give the product as a yellow powder. Yield: 0.083 g, 0.20 mmol, 88% (Found: C, 46.8; H, 5.0; N, 18.8. Calc. for $C_{17}H_{21}N_6BRu$: C, 46.4; H, 4.8; N, 18.9). Mass spectrum: m/z 442 $[M]^+$. Infrared: $\nu(BH)$ 2457, $\nu(CH_{endo})$ 2952, $\nu(CH_{exo})$ 2778 cm^{-1} .

[Ru(η^5 -1,4-ⁱPr₂C₆H₃){κ³-HB(Pz)₃}] 9. [Ru(η^6 -1,4-ⁱPr₂C₆H₄){κ³-HB(Pz)₃}] $[PF_6]$ (0.132 g, 0.21 mmol) was suspended in

degassed thf (15 cm³) and treated with Na[BH₄] (0.05 g, excess). The mixture was refluxed for 2 h then filtered and evaporated to dryness. The crude residue was extracted with diethyl ether, filtered through Celite and evaporated to dryness. Yield: 0.083 g, 0.18 mmol, 82% (Found: C, 53.7, H, 4.6; N, 17.4. Calc. for $C_{21}H_{28}N_6BRu$: C, 54.0, H, 4.1; N, 18.0%). Mass spectrum: m/z 477 $[M - H]^+$. Infrared: $\nu(BH)$, 2473.

[Ru(η^5 -1,3,5-Me₃C₆H₄){κ³-HB(Pz)₃}] 10. [Ru(η^6 -1,3,5-Me₃-C₆H₃){κ³-HB(Pz)₃}] $[PF_6]$ (0.132 g, 0.21 mmol) was suspended in degassed diethyl ether (15 cm³) and treated with Na[BH₄] (0.05 g, excess). The mixture was refluxed for 2 h then filtered and evaporated to dryness. The crude residue was extracted with chloroform, filtered through Celite and evaporated to dryness. Yield: 0.071 g, 0.12 mmol, 59% (Found: C 50.1, H 5.1, N, 20.1. Calc. for $C_{18}H_{23}N_6BRu$: C 49.7, H, 5.3, N, 19.3%). Mass spectrum: m/z 436 $[M]^+$. Infrared: $\nu(BH)$ 2468, $\nu(CH_{endo})$ 2950, $\nu(CH_{exo})$ 2785 cm^{-1} .

[Ru(η^5 -C₆H₆CN){κ³-HC(Pz)₃}] 11. [Ru(η^6 -C₆H₆){κ³-HC(Pz)₃}] $[PF_6]_2$ (0.091 g, 0.13 mmol) was suspended in degassed thf (15 cm³) and treated with KCN (0.05 g, excess). The mixture was refluxed for 3 d then filtered and evaporated to dryness. The crude residue was extracted with chloroform, filtered through Celite and evaporated to dryness. Yield: 0.056 g, 0.10 mmol, 74% (Found: C, 36.1; H, 2.6; N, 17.1. Calc. for $C_{17}H_{16}N_7BF_6PRu$: C, 36.2; H, 2.9; N, 17.4%). Mass spectrum: m/z 420 $[M - PF_6]^+$, 394 $[M - CN - PF_6]^+$. Infrared: $\nu(CH_{endo})$ 2963 cm^{-1} .

[Ru(η^5 -1-ⁱPr-4-MeC₆H₄CN){κ³-HC(Pz)₃}] 12a and 12b. [Ru(η^6 -1-ⁱPr-4-MeC₆H₄){κ³-HC(Pz)₃}] $[PF_6]_2$ (0.122 g, 0.16 mmol) was suspended in degassed thf (15 cm³) and treated with KCN (0.05 g, excess). The mixture was refluxed for 3 d then filtered and evaporated to dryness. The crude residue was extracted with chloroform, filtered through Celite and evaporated to dryness. The two isomers of **12** were not separated. Yield: 0.0786 g, 0.11 mmol, 65% (Found: C 40.8; H 4.0; N 15.4. Calc. for $C_{21}H_{24}N_7F_6PRu$: C 40.7; H 3.9, N 15.8%). Mass spectrum: m/z 476 $[M - PF_6]^+$. Infrared: $\nu(CH_{endo})$ 2915, $\nu(CN)$ 2224 cm^{-1} .

[Ru(η^5 -1,4-Me₂C₆H₄CN){κ³-HC(Pz)₃}] 13. [Ru(η^6 -1,4-Me₂C₆H₄){κ³-HC(Pz)₃}] $[PF_6]_2$ (0.108 g, 0.15 mmol) was suspended in degassed thf (15 cm³) and treated with KCN (0.05 g, excess). The mixture was refluxed for 3 d, then filtered and evaporated to dryness. The crude residue was extracted with chloroform, filtered through Celite and evaporated to dryness. Yield: 0.067 g, 0.11 mmol, 74% (Found: C, 36.7; H, 2.9; N, 17.6. Calc. for $C_{19}H_{20}N_7F_6PRu$: C, 36.2; H, 2.9; N, 17.4%). Mass spectrum: m/z 395 $[M - PF_6]^+$. Infrared: $\nu(CH_{endo})$ 2926, $\nu(CN)$ 2218 cm^{-1} .

[Ru(η^5 -C₆H₇){κ³-HB(3,5-Me₂Pz)₃}] 14. [Ru(η^6 -C₆H₆){κ³-HB(3,5-Me₂Pz)₃}] $[PF_6]$ (0.05 g, 0.08 mmol) was dissolved in thf (10 cm³) and treated with Na[BH₄] (0.05 g, excess). The mixture was stirred at room temperature for 1 h. The red solution was filtered through Celite and evaporated to dryness, giving **14** as a dark residue. Purification was carried out by passing a thf solution of the residue down an alumina column and subsequently evaporating the eluate to dryness. Yield: 0.03 g, 0.06 mmol, 68%. Accurate analytical data could not be obtained due to instability however NMR data are consistent with the proposed formulation. Infrared: $\nu(BH)$ 2538, $\nu(CH_{exo})$ 2798, $\nu(CH_{endo})$ 2924 cm^{-1} .

Crystallography

Crystal data for [Ru(η^5 -C₆H₆CN){κ³-HC(Pz)₃}] $[PF_6]$ ·Me₂CO $C_{20}H_{22}F_6N_7OPRu$, $M = 622.49$, triclinic, space group $P\bar{1}$,

$a = 10.720(5)$, $b = 11.186(4)$, $c = 11.821(3)$ Å, $\alpha = 64.56(3)$, $\beta = 71.43(3)$, $\gamma = 77.97(3)^\circ$, $U = 1209.2(9)$ Å³ (by least squares refinement of diffractometer angles for 25 centred reflections in the range $17.0 < 2\theta < 26.8^\circ$), $\lambda = 0.71073$ Å, $Z = 2$, $F(000) = 624$, $D_c = 1.71$ g cm⁻³, $\mu(\text{Mo-K}\alpha) = 7.89$ cm⁻¹, yellow crystal, $0.30 \times 0.23 \times 0.25$ mm.

The ω - 2θ technique was used to measure 4404 reflections (4176 unique) in the range $5 \leq 2\theta \leq 50^\circ$ at 20 °C. Data were corrected for Lorentz polarisation and absorption effects (Ψ scan method). The structure was solved by conventional direct methods.¹³ and developed by using alternating cycles of least squares refinement and difference-Fourier synthesis.¹⁴ In the final stages of refinement the presence of an acetone of solvation became apparent. The solvent molecule was best modelled as having a two-fold disorder along one of the carbon-carbon bonds such that two sites in the acetone were modelled as a 50:50 mixture of carbon and oxygen atoms. All non-hydrogen atoms, except those involved in the disorder, were modelled anisotropically. Hydrogen atoms on the complex cation were placed in idealised positions and assigned a common isotropic thermal parameter ($U_{\text{iso}} = 0.08$ Å²). The hydrogens of the disordered solvent were omitted. The final cycle of least squares refinement included 315 parameters for 4172 variables and did not shift any parameter by more than 0.001 times its standard deviation. The final R values were $R = 0.0773$, $R' = 0.185$ (for data with $I > 2\sigma(I)$, refinement based on F) and $R = 0.109$, $R' = 0.204$ (for all unique reflections, refinement based on F^2), and the final difference-fourier was featureless with no peaks greater than $1.05 \text{ e} \text{ \AA}^{-3}$.

CCDC reference number 186/1151.

Computation

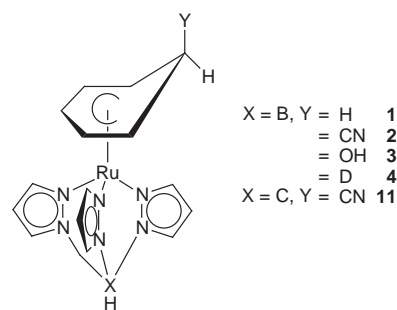
All of the calculations reported in this work were performed at the extended Hückel level of approximation, using the computer aided composition of atomic orbitals (CACAO) package due to Mealli and Proserpio.¹⁵ These programs employ standard extended Hückel methodology,¹⁶ with the weighted H_{ij} formula.¹⁷ Mulliken population analyses were performed.¹⁸ Bond lengths and angles were taken from crystal structure data where available, and idealised to provide the highest possible symmetry.

Results and discussion

Experimental studies

Nucleophilic attack on coordinated benzene. Treatment of a suspension of $[\text{Ru}(\eta^6\text{-C}_6\text{H}_6)\{\kappa^3\text{-HB}(\text{Pz})_3\}][\text{PF}_6]$ in tetrahydrofuran with $\text{Na}[\text{BH}_4]$ results in formation of a yellow solution, which upon work-up leads to isolation of $[\text{Ru}(\eta^5\text{-C}_6\text{H}_6)\{\kappa^3\text{-HB}(\text{Pz})_3\}]$ **1** as an air-sensitive, yellow solid in moderate yield. Similar reactions of $[\text{Ru}(\eta^6\text{-C}_6\text{H}_6)\{\kappa^3\text{-HB}(\text{Pz})_3\}][\text{PF}_6]$ with KCN or KOH give the cyanocyclohexadienyl and hydroxycyclohexadienyl derivatives $[\text{Ru}(\eta^5\text{-C}_6\text{H}_6\text{X})\{\kappa^3\text{-HB}(\text{Pz})_3\}]$, X = CN **2**, OH **3**. While **2** is remarkably stable in solution the corresponding solutions of **1** and **3** change from yellow to green in a few minutes and eventually deposit intractable dark solids. The infrared spectrum of **1** displays two strong bands, at 2963 and 2782 cm⁻¹, which are assigned as $\nu(\text{CH}_{\text{endo}})$ and $\nu(\text{CH}_{\text{exo}})$ respectively.^{19,20} The latter band is absent in the spectra of **2** and **3**, although additional bands are observed at 3450 and 2214 cm⁻¹ (due to $\nu(\text{OH})$ **3** and $\nu(\text{CN})$ **2**). Reaction of $[\text{Ru}(\eta^6\text{-C}_6\text{H}_6)\{\kappa^3\text{-HB}(\text{Pz})_3\}][\text{PF}_6]$ with $\text{Na}[\text{BD}_4]$ gives the deuteriocyclohexadienyl $[\text{Ru}(\eta^5\text{-C}_6\text{H}_6\text{D})\{\kappa^3\text{-HB}(\text{Pz})_3\}]$ **4** which exhibits a $\nu(\text{CH}_{\text{endo}})$ band at 2933 cm⁻¹, no band at ca. 2750–2800 cm⁻¹, and the $\nu(\text{CD}_{\text{exo}})$ band at 2088 cm⁻¹. These observations confirm that the entering nucleophile does so along an *exo* reaction pathway.²¹

The room temperature ¹H NMR spectrum of **1** exhibits five sharp signals for the cyclohexadienyl ligand over a wide range



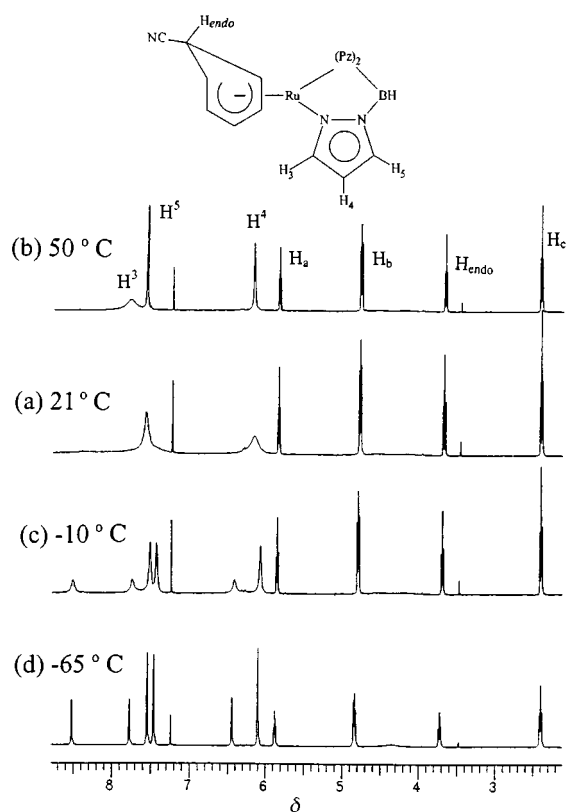
of chemical shifts (δ 5.67 (t), 4.55 (t), 2.73 (t), 2.14 (m) and 2.11 (d)). The appearance of the signals for H_{exo} as a widely spaced doublet ($^2J = 13.3$ Hz) and H_{endo} as a multiplet is consistent with the related resonances reported for the [2.2]paracyclophane derivative $[\text{Ru}(\eta^5\text{-C}_6\text{H}_7)(\eta^6\text{-C}_{16}\text{H}_{16})]^+$.¹ The ¹H NMR spectra (Table 1) of **2–4** are closely similar to that of **1** except that the resonance for H_{exo} is absent in each of the spectra and the signals due to H_{endo} now appear as triplets. While there is nothing remarkable about the cyclohexadienyl signals for any of these compounds, the pyrazolyl regions of the ¹H NMR spectra of **1–4** are quite intriguing. While integration of the two sets of signals confirm the 1:1 stoichiometry of the ligands, and is consistent with the proposed formulations, the signals for the pyrazolyl protons do not appear as three sharp resonances similar to those observed for $[\text{Ru}(\eta^6\text{-C}_6\text{H}_6)\{\kappa^3\text{-HB}(\text{Pz})_3\}][\text{PF}_6]$ (δ 8.67 H³, 6.44 H⁴ 7.87 H⁵).¹⁰ For instance at room temperature the spectrum of **2** exhibits only two broad pyrazolyl resonances (δ 7.58 and 6.16, integral 2:1). However on warming the sample to 50 °C three broad signals become apparent (Fig. 1, δ 7.77 H³, 7.57 H⁵, 6.17 H⁴). Conversely if the temperature of the NMR probe is lowered the broad signals begin to split into two subsets, each of three signals, at around -20 °C and further lowering of the temperature results in the sharpening of these resonances such that at -65 °C there are two well defined sets of resonances (δ 8.52, 7.77, 6.44 and δ 7.54, 7.46, 6.10) in integral ratio 1:2 (Fig. 1). It is notable that throughout this temperature range the signals due to the cyclohexadienyl ligand remain invariant. These observations are repeated for compounds **1**, **3** and **4** with no significant difference in temperature for coalescence. The ¹³C-¹H NMR spectra of **2** (Fig. 2) show a similar pattern of behaviour with the cyclohexadienyl resonances appearing sharp at all temperatures while the broad signals at around 20 °C are replaced by sharp resonances on cooling to -65 °C. At the lower temperature the signals due to carbons in the 3 and 4 positions on the pyrazolyl rings are clearly split (Table 2) while only in the case of the hydroxycyclohexadienyl **3** is the resonance for the carbon in the 5 position resolved. This is quite reasonable given the greater displacement of that carbon atom from the asymmetric ligand.

If the dicationic complex $[\text{Ru}(\eta^6\text{-C}_6\text{H}_6)\{\kappa^3\text{-HC}(\text{Pz})_3\}][\text{PF}_6]_2$ is reacted with KCN a new cyclohexadienyl compound $[\text{Ru}(\eta^5\text{-C}_6\text{H}_6\text{CN})\{\kappa^3\text{-HC}(\text{Pz})_3\}][\text{PF}_6]$ **11** is formed, which is closely analogous to **2**. Variable temperature NMR studies on this compound produce spectra which closely mimic those of the pyrazolylborate derivatives. Clearly these results indicate that the five compounds described so far undergo some kind of fluxional process which in the fast exchange regime average the three pyrazolyl environments yet at lower temperatures render one of the three pyrazolyl groups in the tris(pyrazolyl)borate or tris(pyrazolyl)methane ligand as unique. At first sight it is tempting to attribute these observations to the $[\text{HX}(\text{Pz})_3]^{n+}$ (X = B, $n = 0$; X = C, $n = 1$) ligand undergoing an hapticity change between κ^3 and κ^2 coordination modes, as has been observed for a number of rhodium complexes.^{22,23} However we do not believe that this process is occurring here, as attempts to trap a complex with a κ^2 coordinated ligand, by placing **1** or **11** in solution in the presence of carbon monoxide or $\text{P}(\text{OME})_3$, were unsuccessful. In addition we have previously reported¹¹

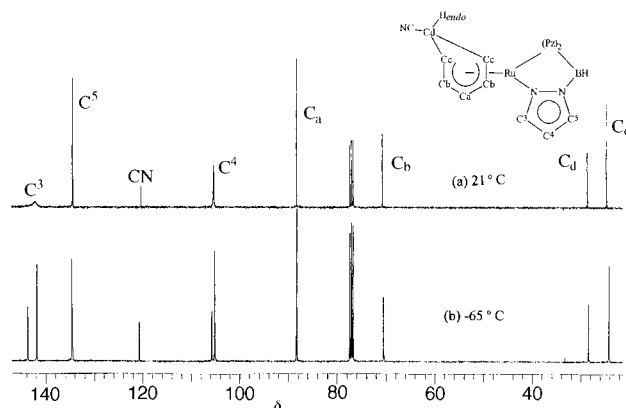
Table 1 Selected ^1H NMR data on non-alkylated ruthenium(cyclohexadienyl)hydridotris(pyrazolyl)-borate and -methane compounds

	Pyrazolyl borate (δ , J/Hz), CDCl_3			Additional resonances
	3-	4-	5-	
$[\text{Ru}(\eta^5\text{-C}_6\text{H}_7)\{\kappa^3\text{-HB}(\text{Pz})_3\}] \mathbf{1}$ -65 °C	8.83 (b, 1H, Pz ¹), 7.53 (s, 2H, Pz ²)	6.45 (b, 1H, Pz ¹), 6.07 (dd, 2H, Pz ²)	7.78 (b, 1H, Pz ¹), 7.46 (d, 2H, Pz ²)	Cyclohexadienyl: 5.71 (t, 1H, $^3J = 4.24$, H _a), 4.62 (t, 2H, $^3J = 5.56$, H _b), 2.74 (m, 1H, $^2J = 12.98$, $^3J = 5.64$, H _{endo}), 2.14 (t, 2H, $^3J = 6.07$, H _c), 2.07 (d, 1H, $^3J = 13.33$, H _{exo}).
$[\text{Ru}(\eta^5\text{-C}_6\text{H}_6\text{CN})\{\kappa^3\text{-HB}(\text{Pz})_3\}] \mathbf{2}$ -65 °C	8.52 (d, 1H, $J = 1.11$, Pz ¹) 7.54 (d, 2H, $J = 2.02$, Pz ²)	6.44 (b, 1H, Pz ¹) 6.10 (b, 2H, Pz ²)	7.77 (d, 1H, $J = 2.11$, Pz ¹) 7.46 (d, 2H, $J = 1.45$, Pz ²)	Cyclohexadienyl: 5.87 (t, 1H, $^3J = 4.57$, H _a), 4.83 (t, 2H, $^3J = 5.51$, H _b), 3.72 (t, 1H, $^3J = 6.10$, H _{endo}), 2.39 (t, 2H, $^3J = 6.05$, H _c).
$[\text{Ru}(\eta^5\text{-C}_6\text{H}_6\text{OH})\{\kappa^3\text{-HB}(\text{Pz})_3\}] \mathbf{3}$ -65 °C	8.60 (b, 1H, Pz ¹) 7.55 (d, 2H, $J = 1.00$, Pz ²)	6.43 (b, 1H, Pz ¹) 6.12 (b, 2H, Pz ²)	7.76 (d, 1H, $J = 1.95$, Pz ¹) 7.53 (b, 2H, Pz ²)	Cyclohexadienyl: 5.62 (t, 1H, $^3J = 4.42$, H _a), 4.80 (t, 2H, $^3J = 6.00$, H _b), 3.68 (t, 1H, $^3J = 5.71$, H _{endo}), 2.72 (t, 2H, $^3J = 5.89$, H _c).
$(\eta[\text{Ru}(\eta^5\text{-C}_6\text{H}_6\text{D})\{\kappa^3\text{-HB}(\text{Pz})_3\}]) \mathbf{4}$ 21 °C	7.56 (b, 6H) ^a	6.11 (b, 3H)	7.56 (b, 6H) ^a	Cyclohexadienyl: 5.66 (t, 1H, $^3J = 4.44$, H _a), 4.55 (t, 2H, $^3J = 5.68$, H _b), 2.71 (t, 1H, $^3J = 6.00$, H _{endo}), 2.12 (t, 2H, $^3J = 6.09$, H _c).
$[\text{Ru}(\eta^5\text{-C}_6\text{H}_6\text{CN})\{\kappa^3\text{-HC}(\text{Pz})_3\}]$ - $[\text{PF}_6] \mathbf{11}$ 21 °C	8.41 (b, 6H) ^a	6.64 (b, 3H)	8.41 (b, 6H) ^a	9.41 [s, 1H, HC(Pz) ₃], cyclohexadienyl: 6.16 (t, 1H, $^3J = 6.9$, H _a), 5.34 (t, 2H, $^3J = 4.8$, H _b), 4.13 (t, 1H, $^3J = 6.09$, H _{endo}), 2.80 (t, 2H, $^3J = 6.06$, H _c).

Pz¹ = unique pyrazolyl group, Pz² = doubly degenerate pyrazolyl group, s = singlet, d = doublet, b = broad, t = triplet, m = multiplet. ^a Broad overlapping signals.

**Fig. 1** Variable temperature ^1H NMR spectra for **2**.

a range of complexes of the type $[\text{Ru}(\eta^6\text{-arene})\{\kappa^2\text{-HX}(\text{Pz})_3\}\text{-Cl}]^{n+}$ ($\text{X} = \text{B}$, $n = 0$; $\text{X} = \text{C}$, $n = 1$) in which the presence of the κ^2 coordinated ligand is conclusively established by X-ray crystallography. These compounds show a quite different chemical shift for the H³ proton on the unique pyrazolyl ring, reinforcing the conclusion that some other process must be operating. Interestingly the crystal structure of **11** (Fig. 3) clearly demonstrates that in the solid state the complex ion adopts a conformation in which one pyrazolyl ring is eclipsed with the projection of the sp³ hybridised carbon atom (torsion angle N12-Ru-centroid-C4 = 2°) and the remaining two

**Fig. 2** Variable temperature $^{13}\text{C}\{-^1\text{H}\}$ NMR spectra for **2**.

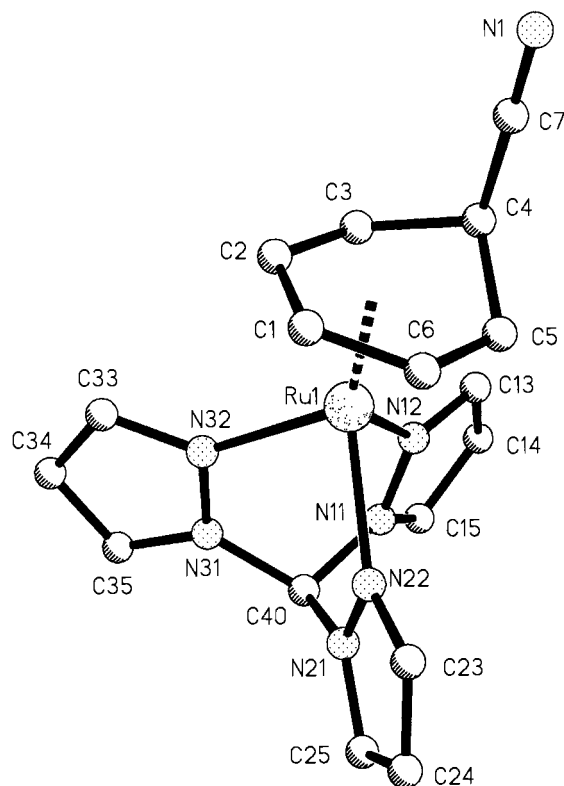
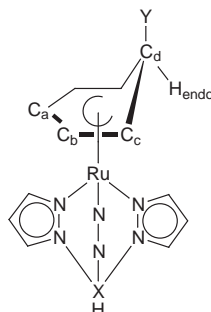
crystallographically unique rings are pseudo-eclipsed with two carbons of the cyclohexadienyl (N22-Ru-centroid-C6 = 10°, N32-Ru-centroid-C2 = 14.2°). Such a structure is clearly consistent with that implied by the low temperature solution NMR data and this measurement has the advantage over the previously reported structure for **2** in that there is no crystallographically imposed symmetry in **11**. The bond lengths in the cation are quite normal (Table 3), with the Ru-N distances being indistinguishable from each other, 2.129(7)–2.136(7) Å, the bonds from the metal to the cyclohexadienyl ligand falling in the range 2.111(9)–2.156(10) Å, and the Ru to sp³ carbon distance being 2.7 Å.

As there is no experimental evidence for Ru-N bond rupture and the establishment of a $\kappa^2 \leftrightarrow \kappa^3$ interconversion, an alternative explanation for the dynamic NMR behaviour must be found. The only logical alternative would seem to be that at low temperature there is restricted rotation of one of the ligands about the metal-ligand axis. Although in principle either ligand could rotate about that axis it seems more logical to suggest that it is the π -bound ligand which would be able to do this without destabilising the complex. While it would be very difficult to establish conclusively by experiment that this process was taking place, the likelihood of such a mechanism operating can be probed computationally. We have therefore conducted a series of extended Hückel molecular orbital calculations to

Table 2 Selected ^{13}C - $\{^1\text{H}\}$ NMR data on non-alkylated ruthenium(cyclohexadienyl)hydridotris(pyrazolyl)-borate and -methane compounds^a

	Pyrazolyl borate (δ) CDCl_3			Additional resonances				
	3-	4-	5-	C_a	C_b	C_c	C_d	CN
$[\text{Ru}(\eta^5\text{-C}_6\text{H}_7)\{\kappa^3\text{-HB}(\text{Pz})_3\}] \mathbf{1}$ -65 °C	143.47 (Pz^1) 141.97 (Pz^2)	104.87 (Pz^1) 105.38 (Pz^2)	134.41	88.78	67.40	26.67	27.78	—
$[\text{Ru}(\eta^5\text{-C}_6\text{H}_6\text{CN})\{\kappa^3\text{-HB}(\text{Pz})_3\}] \mathbf{2}$ -65 °C	145.75 (Pz^1) 141.81 (Pz^2)	105.71 (Pz^1) 105.13 (Pz^2)	134.58	88.26	70.42	24.07	28.30	120.65
$[\text{Ru}(\eta^5\text{-C}_6\text{H}_6\text{OH})\{\kappa^3\text{-HB}(\text{Pz})_3\}] \mathbf{3}$ -65 °C	142.20 (Pz^1) 141.99 (Pz^2)	105.44 (Pz^1) 105.13 (Pz^2)	134.67 (Pz^1) 134.54 (Pz^2)	88.21	68.80	31.47	29.84	—
$[\text{Ru}(\eta^5\text{-C}_6\text{H}_6\text{CN})\{\kappa^3\text{-HC}(\text{Pz})_3\}][\text{PF}_6] \mathbf{11}$ 21 °C	134.49	89.81	109.10	76.64	72.59	28.07	27.83	147.50

^a Pz^1 = unique pyrazolyl group, Pz^2 = doubly degenerate pyrazolyl group.

**Fig. 3** Crystal structure of the cation in **11**.

evaluate this hypothesis, and the results of these studies are discussed below.

Nucleophilic attack on substituted arenes. If the cyclohexadienyl ligands generated in the reactions discussed above do undergo restricted rotation about their Ru–ligand axis then it seems reasonable to suggest that such a process be influenced by the identity of any substituent on the arene ring. To probe this feature of the chemistry we have reacted a range of $[\text{Ru}(\eta^6\text{-arene})\{\text{HB}(\text{Pz})_3\}][\text{PF}_6]$ compounds (arene = 1-ⁱPr-4-MeC₆H₄, 1,4-Me₂C₆H₄, 1,4-ⁱPr₂C₆H₄ or 1,3,5-Me₃C₆H₃) with

Table 3 Selected bond lengths (Å) and angles (°) for $[\text{Ru}(\eta^5\text{-C}_6\text{H}_6\text{CN})\{\kappa^3\text{-HC}(\text{Pz})_3\}][\text{PF}_6]\cdot\text{Me}_2\text{CO} \mathbf{11}$

Ru(1)–C(2)	2.111(9)	Ru(1)–C(6)	2.119(9)
Ru(1)–N(32)	2.136(7)	Ru(1)–N(22)	2.129(7)
Ru(1)–N(12)	2.130(6)	Ru(1)–C(5)	2.146(9)
Ru(1)–C(3)	2.153(9)	Ru(1)–C(1)	2.156(10)
C(1)–C(6)	1.38(2)	C(1)–C(2)	1.44(2)
C(2)–C(3)	1.39(2)	C(3)–C(4)	1.503(14)
C(4)–C(7)	1.488(14)	C(4)–C(5)	1.494(13)
C(5)–C(6)	1.411(14)	C(7)–N(1)	1.142(13)
N(11)–N(12)	1.340(9)	N(11)–C(15)	1.341(10)
N(11)–C(40)	1.446(10)	N(12)–C(13)	1.329(10)
C(13)–C(14)	1.378(13)	C(14)–C(15)	1.353(14)
N(21)–C(25)	1.341(11)	N(21)–N(22)	1.352(9)
N(21)–C(40)	1.434(11)	N(22)–C(23)	1.317(11)
C(23)–C(24)	1.383(13)	C(24)–C(25)	1.366(14)
N(31)–C(35)	1.337(11)	N(31)–N(32)	1.347(9)
N(31)–C(40)	1.446(10)	N(32)–C(33)	1.340(10)
C(33)–C(34)	1.342(14)	C(34)–C(35)	1.366(13)
N(32)–Ru(1)–N(22)	83.6(3)	N(32)–Ru(1)–N(12)	82.4(2)
N(22)–Ru(1)–N(12)	82.9(2)	C(6)–C(1)–C(2)	117.3(9)
C(2)–C(3)–C(4)	118.2(9)	C(4)–C(3)–Ru(1)	93.5(6)
C(7)–C(4)–C(5)	113.1(8)	C(7)–C(4)–C(3)	114.2(9)
C(5)–C(4)–C(3)	102.7(7)	C(6)–C(5)–C(4)	118.0(9)
C(1)–C(6)–C(5)	120.0(9)	N(1)–C(7)–C(4)	178.6(12)
N(12)–N(11)–C(15)	111.4(7)	N(12)–N(11)–C(40)	119.4(6)
C(15)–N(11)–C(40)	129.1(8)	N(11)–N(12)–C(13)	105.9(7)
N(11)–N(12)–Ru(1)	119.3(5)	C(13)–N(12)–Ru(1)	134.6(6)
N(12)–C(13)–C(14)	109.5(8)	C(15)–C(14)–C(13)	106.9(7)
N(11)–C(15)–C(14)	106.3(8)	C(25)–N(21)–N(22)	111.8(7)
C(25)–N(21)–C(40)	127.7(8)	N(22)–N(21)–C(40)	120.4(6)
C(23)–N(22)–N(21)	105.1(7)	C(23)–N(22)–Ru(1)	136.7(6)
N(21)–N(22)–Ru(1)	118.2(5)	N(22)–C(23)–C(24)	111.0(9)
C(25)–C(24)–C(23)	105.8(8)	N(21)–C(25)–C(24)	106.2(8)
C(35)–N(31)–N(32)	112.2(7)	C(35)–N(31)–C(40)	128.2(8)
N(32)–N(31)–C(40)	119.6(6)	C(33)–N(32)–N(31)	103.9(7)
C(33)–N(32)–Ru(1)	137.2(6)	N(31)–N(32)–Ru(1)	118.9(5)
N(32)–C(33)–C(34)	111.4(8)	C(33)–C(34)–C(35)	106.9(8)
N(31)–C(35)–C(34)	105.6(9)	N(21)–C(40)–N(31)	111.9(6)
N(21)–C(40)–N(11)	110.1(6)	N(31)–C(40)–N(11)	109.2(7)

nucleophiles and subjected the products to variable temperature NMR studies (Tables 4 and 5).

Reaction of $[\text{Ru}(\eta^6\text{-1-}^i\text{Pr-4-MeC}_6\text{H}_4)\{\text{HB}(\text{Pz})_3\}][\text{PF}_6]$ with $\text{Na}[\text{BH}_4]$ in tetrahydrofuran at room temperature results in the formation of two isomeric products $[\text{Ru}(\eta^5\text{-1-}^i\text{Pr-4-}$

Table 4 Selected ¹H NMR data on alkylated ruthenium(cyclohexadienyl)hydriotris(pyrazole)-borate and -methane compounds

		Pyrazoyl borate (δ , J/Hz) CDCl ₃			Cyclohexadienyl resonances
		3-	4-	5-	
[Ru(η^5 -1- ⁱ Pr-4-MeC ₆ H ₅){ κ^3 -HB(Pz) ₃ }] 5a + 5b –65 °C	Isomer a	8.89, 7.93, 7.70	6.50, 6.11, 6.04	7.99, 7.69, 7.46	Isomer a : δ 5.49 and 4.56 (d, 2H, ³ J = 4.4, AB), 2.68 (m, 1H, ² J = 12.4, ³ J = 6.8, H _{endo}), 2.46 (sep, 1H, ³ J = 6.8, ¹ Pr), 2.15 (d, 1H, ² J = 12.4, H _{exo}), 1.79 (d, 1H, ³ J = 6.0, H _c), 0.93 (s, 3H, Me), 0.74 (d, 3H, ³ J = 6.8, ¹ Pr), 0.32 (d, 3H, ³ J = 6.8, ¹ Pr).
	Isomer b	8.91, 7.93, 7.71	6.53, 6.12, 6.06	7.99, 7.69, 7.64	Isomer b : 5.54 and 4.58 (d, 2H, ³ J = 4.4, AB), 2.77 (m, 1H, ² J = 12.4, ³ J = 6.8, H _{endo}), 1.77 (sep, 1H, ³ J = 6.8, ¹ Pr), 2.05 (d, 1H, ² J = 12.4, H _{exo}), 2.04 (s, 3H, Me), 1.88 (d, 1H, ³ J = 6.0, H _c), 1.34 (d, 3H, ³ J = 6.8, ¹ Pr), 1.08 (d, 3H, ³ J = 6.8, ¹ Pr).
[Ru(η^5 -1- ⁱ Pr-4-MeC ₆ H ₄ CN){ κ^3 -HB(Pz) ₃ }] 6a + 6b ^c 21 °C	Isomer a	8.80, 7.87, 7.86	6.46, 6.10, 6.03	7.88, 7.68, 7.58	Isomer a : 5.77 and 4.78 (d, 2H, ³ J = 4.8, AB), 2.60 (sep, 1H, ³ J = 6.8, ¹ Pr), 1.40 (s, 3H, Me), 0.93 (d, 3H, ³ J = 6.8, ¹ Pr), 0.51 (d, 3H, ³ J = 6.8, ¹ Pr).
	Isomer b				Isomer b : 5.78 and 4.73 (d, 2H, ³ J = 4.8, AB), 2.18 (s, 3H, Me), 1.91 (sep, 1H, ³ J = 6.8, ¹ Pr), 1.41 (d, 3H, ³ J = 6.8, ¹ Pr), 1.19 (d, 3H, ³ J = 6.8, ¹ Pr).
[Ru(η^5 -1- ⁱ Pr-4-MeC ₆ H ₄ OH){ κ^3 -HB(Pz) ₃ }] 7a + 7b –65 °C ^{a,b}	Isomer a	8.90, 7.96, 7.34	6.50, 6.18, 6.11	8.07, 7.73, 7.60	Isomer a : 5.57 and 4.93 (d, 2H, ³ J = 4.8, AB), 3.95 (d, 1H, ³ J = 5.6, H _{endo}), 2.68 (sep, 1H, J = 6.8, ¹ Pr), 2.44 (d, 1H, J = 5.6, H _c), 1.31 (d, 3H, J = 6.8, ¹ Pr), 1.31 (s, 3H, Me), 1.18 (d, 3H, J = 6.8, ¹ Pr).
	Isomer b				Isomer b : 5.52 and 5.13 (d, 2H, ³ J = 4.8, AB), 4.81 (d, 1H, ³ J = 5.6, H _{endo}), 4.09 (d, 1H, J = 5.6, H _c), 2.16 (s, 3H, Me), 1.06 (sep, 1H, J = 6.8, ¹ Pr), 1.09 (d, 3H, J = 6.8, ¹ Pr), 0.67 (d, 3H, J = 6.8, ¹ Pr).
[Ru(η^5 -1,4-Me ₂ C ₆ H ₃){ κ^3 -HB(Pz) ₃ }] 8 –80 °C		8.82 (d, 1H, J = 1.6), 7.91 (d, 1H, J = 1.6), 7.73 (d, 1H, J = 2.4)	6.54 (dd, 1H), 6.12 (dd, 1H), 6.07 (dd, 1H)	8.01 (d, 1H, J = 2.0), 7.74 (d, 1H, J = 2.4), 7.68 (d, 1H, J = 2.8)	5.47 and 4.58 (d, 2H, ³ J = 4.4, AB), 2.74 (dd, 1H, ³ J = 5.6, ² J = 12.6, H _{endo}), 2.08 (d, 1H, ² J = 12.6, H _{exo}), 2.05 (s, 3H, Me _a), 1.85 (d, 1H, ³ J = 6, H _c), 0.89 (s, Me _b , 3H).
[Ru(η^5 -1,4- ⁱ Pr ₂ C ₆ H ₃){ κ^3 -HB(Pz) ₃ }] 9 40 °C ^c		8.82, 7.77, 7.56	6.43, 6.05, 6.05	7.83, 7.53, 7.48	5.60 and 4.42 (2H, ³ J = 4.4, AB), 2.74 (m, 1H, ³ J = 6.8, ² J = 12.6, H _{endo}), 2.48 (sep, 1H, ³ J = 6.8, ¹ Pr _a), 2.18 (d, 1H, ² J = 12.8, H _{exo}), 1.95 (d, 1H, ³ J = 6.8, H _c), 1.79 (sep, 1H, ³ J = 6.8, ¹ Pr _b), 1.36 (d, 3H, ³ J = 6.8, ¹ Pr _a), 1.12 (d, 3H, ³ J = 6.8, ¹ Pr _a), 0.77 (d, 3H, ³ J = 6.8, ¹ Pr _b), 0.40 (d, 3H, ³ J = 6.8, ¹ Pr _b).
[Ru(η^5 -1,3,5-Me ₃ C ₆ H ₄){ κ^3 -HB(Pz) ₃ }] 10 21 °C		8.71 (d, 1H, ³ J = 1.6, Pz ¹), 7.74 (d, 2H, ³ J = 1.6, Pz ²)	6.48 (dd, 1H, Pz ¹), 6.08 (dd, 2H, Pz ²)	7.88 (d, 1H, ³ J = 2.4, Pz ¹), 7.58 (d, 2H, ³ J = 2.4, Pz ²)	4.39 (s, 2H, H _a), 2.46 (d, 1H, ² J = 12.8, 6.8, H _{endo}), 2.32 (s, 3H, Me _a), 2.21 (d, 1H, ² J = 12.8, H _{exo}), 1.05 (s, 6H, Me _b).
[Ru(η^5 -1,3,5-Me ₃ C ₆ H ₃ CN){ κ^3 -HB(Pz) ₃ }] 21 °C		8.32 (d, 1H, J = 1.6, Pz ¹), 7.51 (d, 2H, J = 1.6, Pz ²)	6.43 (dd, 1H, Pz ¹), 6.07 (dd, 2H, Pz ²)	7.72 (d, 1H, J = 2.4, Pz ¹), 7.48 (d, 2H, J = 2.4, Pz ²)	4.36 (s, 2H, H _a), 3.28 (s, 1H, H _{endo}), 2.35 (s, 3H, Me _a), 1.18 (s, 6H, Me _b).
[Ru(η^5 -1- ⁱ Pr-4-MeC ₆ H ₄ CN){ κ^3 -HC(Pz) ₃ }] [PF ₆] ^d 12a + 12b ^c 21 °C		9.27, 8.42, 8.33	6.90, 6.54, 6.48	8.59, 8.04, 8.31	9.44 [s, 1H, HC(Pz) ₃], Isomer a : 6.05 (d, 1H, ³ J = 6.3), 5.01 (d, 1H, ³ J = 4.8), 4.04 (d, 1H, ³ J = 6.0, H _{endo}), 1.22 (s, 3H, Me ²), 1.00 (d, 3H, ³ J = 6.9, ¹ Pr ²), 0.60 (d, 3H, ³ J = 6.9, ¹ Pr ²). Isomer b : 6.04 and 5.09 (d, 1H, ³ J = 5.1, AB), 4.04 (d, 1H, ³ J = 6.0), 1.43 (d, 3H, ³ J = 6.6, ¹ Pr), 2.27 (s, 3H, Me ¹), 1.21 (d, 3H, ³ J = 6.6, ¹ Pr ¹).
[Ru(η^5 -1,4-Me ₂ C ₆ H ₄ CN){ κ^3 -HC(Pz) ₃ }] [PF ₆] 13 ^d 21 °C		8.39	6.54	8.37	9.40 [s, 1H, HC(Pz) ₃], cyclohexadienyl: 6.01 and 5.04 (d, 2H, ³ J = 4.0, AB), 4.03 (d, 1H, ³ J = 5.9), 2.65 (s, 1H, ³ J = 6.0, H _c), 2.26 (s, 3H, Me ¹), 1.21 (s, 3H, Me ²).
[Ru(η^5 -C ₆ H ₇){ κ^3 -HB(3,5-Me ₂ Pz) ₃ }] 14 –65 °C		2.87 (s, 3H, Pz ¹), 2.27 (s, 6H, Pz ²)	6.05 (s, 1H, Pz ¹), 5.61 (s, 2H, Pz ²)	2.34 (s, 3H, Pz ¹), 2.19 (s, 6H, Pz ²)	6.16 (t, 1H, ³ J = 4.67, H _a), 5.18 (dd, 2H, ³ J = 5.67, H _b), 2.79 (m, 1H, ² J = 12.82, ³ J = 6.54, H _{endo}), 2.45 (t, 2H, ³ J = 6.08, H _c), 1.51 (d, 1H, ² J = 13.41, H _{exo}).

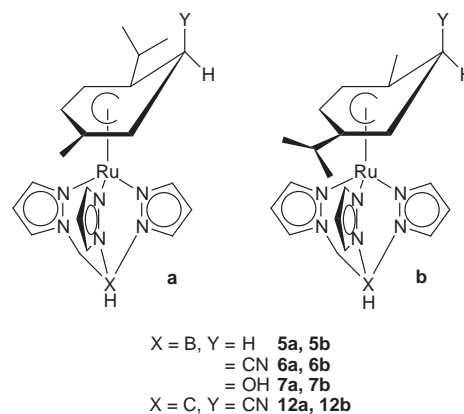
s = singlet, d = doublet, dd = doublet of a doublet, m = multiplet, sep = septet. Pz¹ = unique pyrazoyl group, Pz² = doubly degenerate pyrazoyl group. ^a Isomer **b** pyrazoyl signals at 21 °C appear as broad resonances in the baseline. ^b Only four isomer **b** pyrazoyl signals are clearly seen due to overlap with those of isomer **a** (δ 8.92, 7.99, 7.68, 6.06). ^c All pyrazoyl signals broad and equivalent to 1H. ^d All pyrazoyl signals broad and equivalent to 3H.

Table 5 Selected ^{13}C NMR data on alkylated ruthenium(cyclohexadienyl)hydridotris(pyrazolyl)-borate and -methane compounds

	Pyrazolyl borate (δ) CDCl_3			Additional resonances
	3-	4-	5-	
$[\text{Ru}(\eta^5\text{-1-}^i\text{Pr-4-MeC}_6\text{H}_5)\{\kappa^3\text{-HB(Pz)}_3\}]$ 5a + 5b -70°C	144.10, 143.64, 143.40, 143.15, 142.05, 141.53	135.42, 135.19, 134.96, 134.88, 134.72, 134.53	106.41, 106.11, 105.53, 105.42, 105.33, 105.17	Cyclohexadienyl: 108.91, 99.52, 86.72, 82.90, 67.43, 64.38, 46.75, 36.88, 35.17, 34.00 CH ₂ : 32.55, 32.12 Me and ⁱ Pr: 24.17, 24.02, 23.14, 22.09, 21.95, 21.19, 20.67, 19.70 CN: 121.69, 120.24
$[\text{Ru}(\eta^5\text{-1-}^i\text{Pr-4-MeC}_6\text{H}_4\text{CN})\{\kappa^3\text{-HB(Pz)}_3\}]$ 6a + 6b -21°C	145.51, 143.97, 142.07	106.49, 105.78, 105.46	135.58, 135.25, 135.22	Cyclohexadienyl: 108.99, 99.16, 87.09, 84.58, 70.65, 68.01, 67.43, 44.83, 35.91, 34.29 CHCN: 32.84, 32.05 Me and ⁱ Pr: 24.30, 23.88, 22.76, 21.84, 21.73, 21.13, 20.96, 20.15
$[\text{Ru}(\eta^5\text{-1,4-Me}_2\text{C}_6\text{H}_5)\{\kappa^3\text{-HB(Pz)}_3\}]$ 8 -65°C	143.34, 143.14, 141.59	106.44, 105.53, 105.29	135.33, 134.97, 134.74	Cyclohexadienyl: 99.41, 86.93, 66.92, 35.88, 34.82 CH ₂ : 25.39 Me: 21.90, 22.22
$[\text{Ru}(\eta^5\text{-1,4-}^i\text{Pr}_2\text{C}_6\text{H}_5)\{\kappa^3\text{-HB(Pz)}_3\}]$ 9 -21°C	144.47, 143.64, 142.37	106.07, 105.45, 105.19	135.33, 134.91, 135.59	Cyclohexadienyl: 109.35, 83.88, 65.35, 46.77, 34.48 CH ₂ : 33.16 ⁱ Pr: 32.73, 24.29, 23.20, 21.52, 20.91, 19.84 CN: 119.11
$[\text{Ru}(\eta^5\text{-1,3,5-Me}_3\text{C}_6\text{H}_3\text{CN})\{\kappa^3\text{-HB(Pz)}_3\}]$ -21°C	141.53, 141.22	105.02, 104.96	134.39, 134.29	Cyclohexadienyl: 87.26, 80.06, 40.28 CH ₂ : 33.09 Me: 20.21, 18.38
$[\text{Ru}(\eta^5\text{-C}_6\text{H}_7\text{CN})\{\kappa^3\text{-HB(3,5-Me}_2\text{Pz)}_3\}]$ 14 -65°C	154.04, 17.82 152.27, 16.04	107.92 108.42	143.45, 13.27 143.08, 13.09	Cyclohexadienyl: 81.44, 67.97, 28.20 CH ₂ : 16.04

$\text{MeC}_6\text{H}_5\{\text{HB(Pz)}_3\}$ **5a** and **5b**. The observation of two isomers is not surprising as there are two potential sites of attack on the *para*-cymene ligand, *ortho* to either a methyl or an isopropyl group. Previous work on similar derivatives containing [2.2]paracyclophane as the spectator ligand reported that isomeric form **b** was the more prevalent due to steric effects.¹ However in this study the products are formed in similar quantities. The reactions of $[\text{Ru}(\eta^6\text{-1-}^i\text{Pr-4-MeC}_6\text{H}_4)\{\text{HB(Pz)}_3\}][\text{PF}_6]$ with KCN and NaOH yield the related isomeric derivatives **6a/6b** and **7a/7b**. The introduction of a nucleophile onto *para*-cymene renders the cyclohexadienyl product asymmetric and hence considerably increases the complexity of the room temperature NMR spectrum which is nevertheless consistent with the presence of two isomers of the cyclohexadienyl ligand (Table 4). However once again it is the NMR spectrum of the pyrazolyl protons which are the more intriguing. In the presence of the asymmetric cyclohexadienyl ligand each of the pyrazolyl ring protons is unique, hence each isomer should exhibit nine resonances. Examination of the room temperature ^1H NMR spectrum of **5** reveals only nine somewhat broad signals (δ 8.84, 7.86, 7.77, 7.64, 7.58, 7.55, 6.45, 6.06, and 5.98) indicating a single isomer. However when the $^{13}\text{C}\{-^1\text{H}\}$ NMR spectrum is recorded it is apparent that although there are nine relatively sharp signals there are additional very broad resonances in the base line. Closer examination of the ^1H NMR spectrum reveals several very broad additional resonances which can be attributed to the second isomer. Recording the NMR spectrum of **5** at low temperature conclusively demonstrates that both isomers are present as both the ^1H and $^{13}\text{C}\{-^1\text{H}\}$ spectra clearly show eighteen pyrazolyl environments (Tables 4 and 5).

Our interpretation of these observations is that the two isomers have different barriers to rotation. From our variable temperature NMR experiments it seems that the isomers of type **b** have similar coalescence temperatures to those observed for compounds **1–4** while those for isomeric form **a** are significantly higher. Analogous NMR behaviour has been observed for the tris(pyrazolyl)methane compound $[\text{Ru}(\eta^5\text{-1-}^i\text{Pr-4-MeC}_6\text{H}_4\text{CN})\{\kappa^3\text{-HC(Pz)}_3\}][\text{PF}_6]$ **12a** and **12b**. To attempt to substantiate this deduction we prepared and studied by variable temperature NMR the compounds $[\text{Ru}(\eta^5\text{-1,4-Me}_2\text{C}_6\text{H}_5)\{\kappa^3\text{-HB(Pz)}_3\}]$ **8** and $[\text{Ru}(\eta^5\text{-1,4-}^i\text{Pr}_2\text{C}_6\text{H}_5)\{\kappa^3\text{-HB(Pz)}_3\}]$ **9**. Inspec-



tion of the room temperature ^1H NMR spectrum of **8** reveals seven very broad resonances, two of which each integrate for two protons (Fig. 4) with no resolved coupling in the region δ 6.5–8.9. Cooling of the NMR probe results in a sharpening of the signals down to -40°C , at which point couplings can be clearly observed, with no further changes observed down to -80°C . If the NMR tube is warmed to *ca.* 50°C the spectrum changes such that only two broad resonances, δ 7.66 and 6.12, relative integral 2:1, are observed. Throughout this 130°C temperature range the signals for the cyclohexadienyl ligand remained essentially invariant. By contrast, when the room temperature ^1H NMR spectrum of **9** is recorded nine sharp well defined pyrazolyl proton resonances (Fig. 4) are observed between 20 and 50°C . Related behaviour is observed in the variable temperature $^{13}\text{C}\{-^1\text{H}\}$ NMR spectra of this pair of compounds. The conclusion to be drawn from these observations must clearly be that the barrier to rotation is higher when the site of nucleophilic attack is adjacent to the isopropyl substituent. Hence in the case of compounds **5, 6**, and **7**, it is isomer **a** which is responsible for the sharper signals in the room temperature spectra.

When $\text{Na}[\text{BH}_4]$ is reacted with $[\text{Ru}(\eta^6\text{-1,3,5-Me}_3\text{C}_6\text{H}_3)\{\kappa^3\text{-HB(Pz)}_3\}][\text{PF}_6]$ a single product resulting from the addition of a hydride to an unsubstituted aromatic carbon atom is isolated, $[\text{Ru}(\eta^5\text{-1,3,5-Me}_3\text{C}_6\text{H}_4)\{\kappa^3\text{-HB(Pz)}_3\}]$ **10**. Interestingly the pyrazolyl region of the NMR spectrum displays two sets of sharp

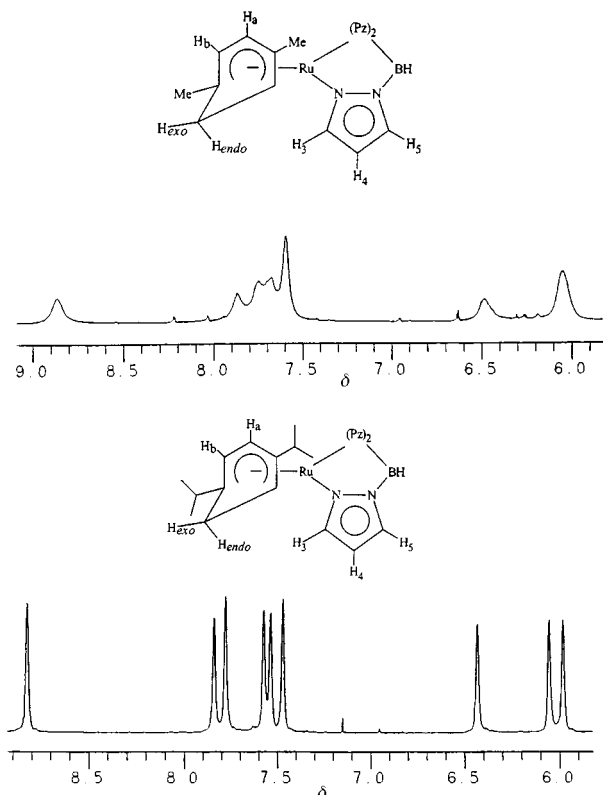
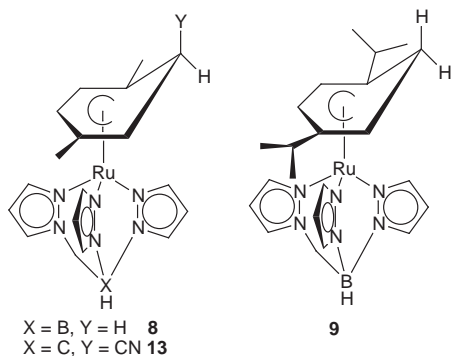


Fig. 4 Part of the ^1H NMR spectra of **8** and **9** recorded at room temperature.



pyrazolyl signals in integral ratio 1:2 (δ 8.71, 7.88, 6.48 and 7.74, 7.58, 6.08). Similarly the resonances observed in the room temperature ^{13}C - $\{^1\text{H}\}$ NMR spectrum (Table 5) are sharp. Clearly these observations are consistent with a high barrier to rotation and perhaps indicate that it is both the identity of the substituents on the cyclohexadienyl ligand, as previously established, and their number which contribute to the height of the rotational barrier.

Finally, each of the experiments described to date has involved unsubstituted pyrazolyl rings. In a final experiment we examined the reaction of the compound $[\text{Ru}(\eta^6\text{-C}_6\text{H}_6)\{\kappa^3\text{-HB}(3,5\text{-Me}_2\text{Pz})_3\}][\text{PF}_6]$, which has substituents on the pyrazolyl

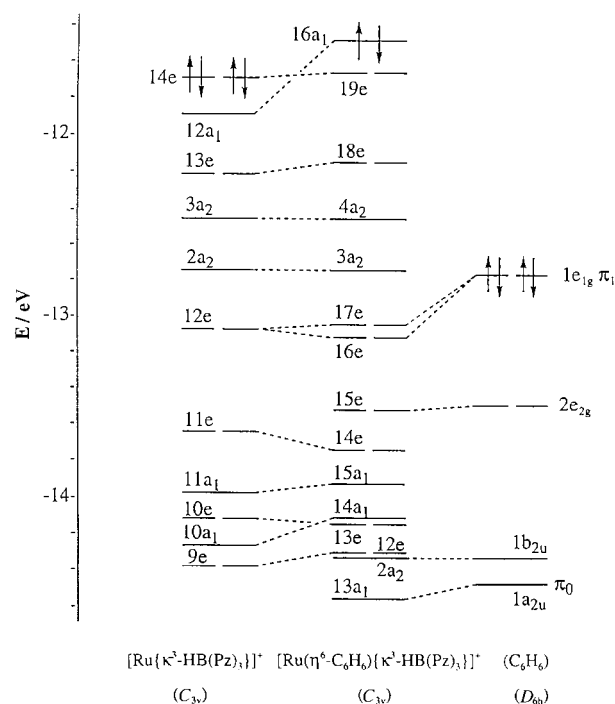
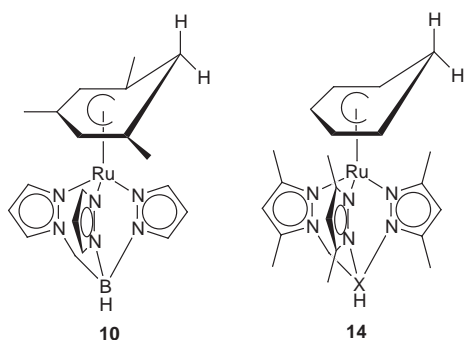


Fig. 5 Fragment EHMO diagram for $[\text{Ru}(\eta^6\text{-C}_6\text{H}_6)\{\kappa^3\text{-HB}(\text{Pz})_3\}]^+$.

rings placed so as to interact with the second ligand, with $\text{Na}[\text{BH}_4]$. This reaction was not particularly clean and good analytical data could not be obtained on the product, $[\text{Ru}(\eta^5\text{-C}_6\text{H}_7)\{\kappa^3\text{-HB}(3,5\text{-Me}_2\text{Pz})_3\}]$ **14**. Nevertheless ^1H and ^{13}C - $\{^1\text{H}\}$ NMR studies reveal that at room temperature the pyrazolyl environments are averaged, due to rapid rotation about the metal–ligand axis, while at low temperature ‘frozen-out’ structure is observed. In the case of this compound the unique pyrazolyl signals in the ^1H NMR spectrum occur at δ 6.05, 2.87 and 2.34, while the doubly degenerate set occur at δ 5.61, 2.27 and 2.19. One might conclude from this observation that, since the barrier appears comparable to that for **1**, the barrier height is determined by the nature of the cyclohexadienyl ligand. This hypothesis is explored further in the calculations described below.

Computational investigations

In order to understand more fully the experimentally observed barriers to rotation of the carbocyclic ligand in **1**, **8**, **9** and **10**, we have carried out a series of extended Hückel molecular orbital (EHMO) calculations on these molecules as well as the parent arene $[\text{Ru}(\eta^6\text{-C}_6\text{H}_6)\{\kappa^3\text{-HB}(\text{Pz})_3\}]^+$.

The electronic structure of $[\text{Ru}(\eta^6\text{-C}_6\text{H}_6)\{\kappa^3\text{-HB}(\text{Pz})_3\}]^+$. A fragment MO energy level diagram for the interaction of a benzene ring with a $[\text{Ru}\{\kappa^3\text{-HB}(\text{Pz})_3\}]^+$ unit is shown in Fig. 5. There are four benzene MOs which lie in the eigenvalue range shown, but only two are expected to interact with the metal fragment. These are the $1a_{2u} \pi_0$ and $1e_{1g} \pi_1$ orbitals, which are the π orbitals with zero and one vertical nodes respectively.²⁴ The $1b_{2u}$ and $2e_{2g}$ levels which lie between the π_0 and π_1 in energy terms are C–C σ antibonding and, in the case of the latter, C–H bonding. They are essentially unaltered on complexation to the $[\text{Ru}\{\kappa^3\text{-HB}(\text{Pz})_3\}]^+$ fragment. Similarly, many of the metal moiety's orbitals are unaffected by the presence of the benzene ring. The principal $[\text{Ru}\{\kappa^3\text{-HB}(\text{Pz})_3\}]^+$ -benzene interaction is in the 16e, 17e and 19e orbitals. The 16e and 17e are mixtures of the $[\text{Ru}\{\kappa^3\text{-HB}(\text{Pz})_3\}]^+$ 12e MOs† with the π_1

† The 12e $[\text{Ru}\{\kappa^3\text{-HB}(\text{Pz})_3\}]^+$ MO is Ru–HB(Pz)₃ bonding, with 16% metal character. The 14e $[\text{Ru}\{\kappa^3\text{-HB}(\text{Pz})_3\}]^+$ HOMO is primarily Ru d-based, with some Ru–HB(Pz)₃ antibonding character, and the 12a₁ $[\text{Ru}\{\kappa^3\text{-HB}(\text{Pz})_3\}]^+$ orbital is almost exclusively Ru d_{z²}.

orbitals of benzene. The 19e MO has contributions from the 14e HOMO of the $[\text{Ru}\{\kappa^3\text{-HB}(\text{Pz})_3\}]^+$ fragment and the unfilled π_2 levels of benzene; it may be regarded as Ru \rightarrow benzene backbonding. The HOMO of $[\text{Ru}(\eta^6\text{-C}_6\text{H}_6)\{\kappa^3\text{-HB}(\text{Pz})_3\}]^+$ is the 16a₁ orbital derived primarily from the 12a₁ MO of $[\text{Ru}\{\kappa^3\text{-HB}(\text{Pz})_3\}]^+$. It is >90% Ru d_{z²} in character.

Rotation of the benzene ring through 120° about the Ru–benzene centroid vector in $[\text{Ru}(\eta^6\text{-C}_6\text{H}_6)\{\kappa^3\text{-HB}(\text{Pz})_3\}]^+$. Although we have no experimental measure of the rotational barrier in $[\text{Ru}(\eta^6\text{-C}_6\text{H}_6)\{\kappa^3\text{-HB}(\text{Pz})_3\}]^+$, other workers have used a variety of techniques to study the barriers in other transition metal–arene systems.²⁵ The rotational barrier in $[\text{Cr}(\eta^6\text{-C}_6\text{H}_6)(\text{CO})_3]$ has been measured by several methods, and estimates range from 15.5–19.7 kJ mol⁻¹ at room temperature to 27.5 kJ mol⁻¹ at 10 K. A value of 1.2 kJ mol⁻¹ for the same compound has been calculated by the extended Hückel approach.²⁶ More recently, variable temperature solid state ²H NMR studies of $[\text{Mo}(\eta^6\text{-C}_6\text{D}_6)_2]$ found that the spectra are invariant in the temperature range 160–360 K, consistent with rapid ring rotation at all accessible temperatures.²⁷ It is therefore highly probable that the barrier in $[\text{Ru}(\eta^6\text{-C}_6\text{H}_6)\{\kappa^3\text{-HB}(\text{Pz})_3\}]^+$ is also very small, and it is important that we are able to reproduce this computationally. Fig. 6 plots the total EHMO energy of $[\text{Ru}(\eta^6\text{-C}_6\text{H}_6)\{\kappa^3\text{-HB}(\text{Pz})_3\}]^+$ as the benzene ring is rotated by 120° in steps of 6°, beginning (and ending) in an eclipsed conformation (Fig. 7). As the benzene fragment is rotated by 120° the total energy passes through two minima (30° and 90°) and one maximum (60°), the energy of the latter being the same as at 0° and 120° of rotation, reflecting the six-fold rotational symmetry of the benzene ring. Fig. 6 reveals that the initial, eclipsed conformation is unstable with respect to the staggered geometry obtained when the ring is rotated by 30° and 90°, and the barrier on moving from staggered \rightarrow eclipsed \rightarrow staggered is 10.6 kJ mol⁻¹. This value is entirely consistent with the experimental data discussed above for $[\text{Cr}(\eta^6\text{-C}_6\text{H}_6)(\text{CO})_3]$ and $[\text{Mo}(\eta^6\text{-C}_6\text{D}_6)_2]$, and is unsurprising in view of the high symmetry of the benzene fragment. Indeed, in treatments of the interactions of planar aromatic carbocyclic ligands with transition metal centres it is common to assume that the metal–ring centroid axis is an infinite axis to rotation.^{28–30} This may be thought of as the σ framework of the ring rotating with the π system remaining fixed. Thus we may conclude that the EHMO calculations predict a very small energy barrier to rotation of the benzene about the Ru–benzene centroid vector, due to the interaction of the benzene π system with the Ru fragment orbitals being essentially unaltered as the ring is rotated.

The electronic structure of 1. A fragment MO diagram for the interaction of C₆H₇⁻ with $[\text{Ru}\{\kappa^3\text{-HB}(\text{Pz})_3\}]^+$ is given in Fig. 8. The orbitals of the cyclohexadienyl fragment are labelled according to the irreducible representation of the C_s point group that they span. It may be seen that, in addition to the 8a' π_0 , 6a'' π_{1b} and 10a' π_{1nb} levels,[‡] there are a further three cyclohexadienyl orbitals in the energy range shown (4a'', 5a'' and 9a'). The 9a' and 5a'' levels are C–C and C–H σ bonding, while the 4a'' orbital is mainly C–C σ antibonding with a smaller C–H bonding component. None of these σ levels interacts to any significant extent with the Ru atom. The principal $[\text{Ru}\{\kappa^3\text{-HB}(\text{Pz})_3\}]^+$ –cyclohexadienyl interaction is concentrated in the 34a' and 20a'' orbitals although there is some $[\text{Ru}\{\kappa^3\text{-HB}(\text{Pz})_3\}]^+$ –cyclohexadienyl orbital mixing in other levels. The 20a'' MO is made up of a mixture of the C₆H₇⁻ 6a'' π_{1b} level and the 13e orbital of the metal fragment, while the 34a' orbital is a combination of C₆H₇⁻ 10a' π_{1nb} and several Ru AOs (d_{z²}, d_{xz} and p_x). The 15e lowest unoccupied MO (LUMO) of the metal fragment (not shown) is also a contributor to this level. The

[‡] The π_{1b} and π_{1nb} MOs are the cyclohexadienyl π orbitals with one vertical node, which are C–C bonding and non-bonding respectively.

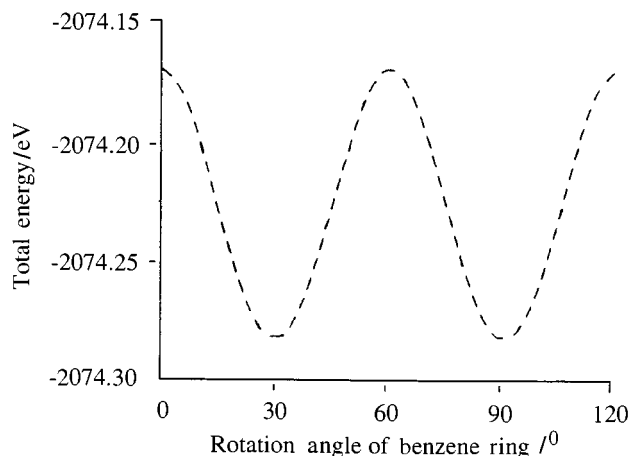


Fig. 6 Variation of the total EHMO energy of $[\text{Ru}(\eta^6\text{-C}_6\text{H}_6)\{\kappa^3\text{-HB}(\text{Pz})_3\}]^+$ as the benzene ring is rotated by 120° in steps of 6°, beginning in an eclipsed conformation.

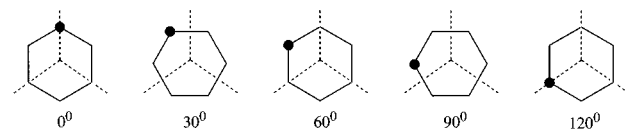


Fig. 7 Rotational motion of the benzene ring around the Ru–ring centroid vector in $[\text{Ru}(\eta^6\text{-C}_6\text{H}_6)\{\kappa^3\text{-HB}(\text{Pz})_3\}]^+$ (---- denotes a Pz ring and ● follows one of the C atoms during the course of the rotation).

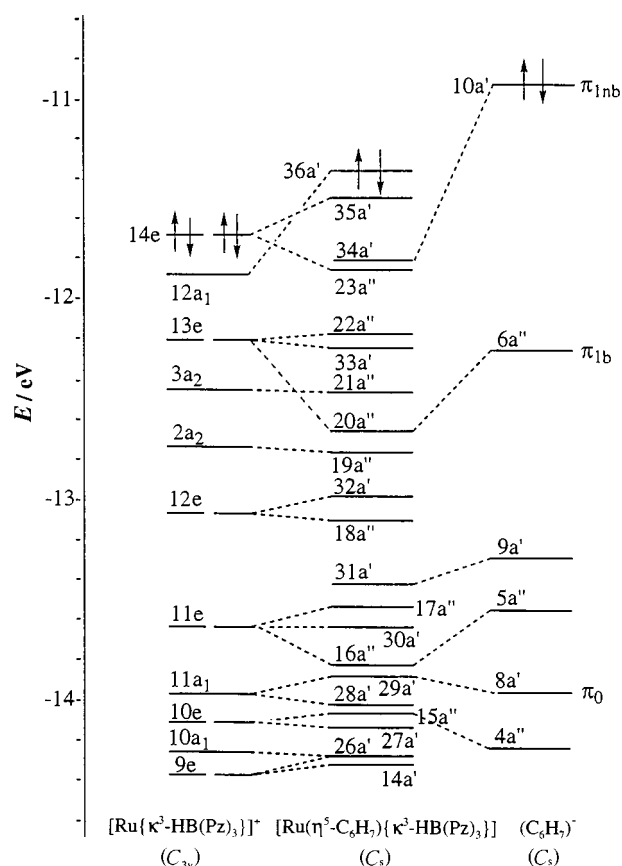


Fig. 8 Fragment EHMO diagram for 1.

36a' HOMO of 1 is largely derived from the 12a₁ MO of the $[\text{Ru}\{\kappa^3\text{-HB}(\text{Pz})_3\}]^+$ unit, and is therefore predominantly Ru d_{z²} in character.

Rotation of the cyclohexadienyl ring through 120° about the Ru–cyclohexadienyl centroid vector in 1. The cyclohexadienyl ring of 1 was rotated by 120° in a manner analogous to the

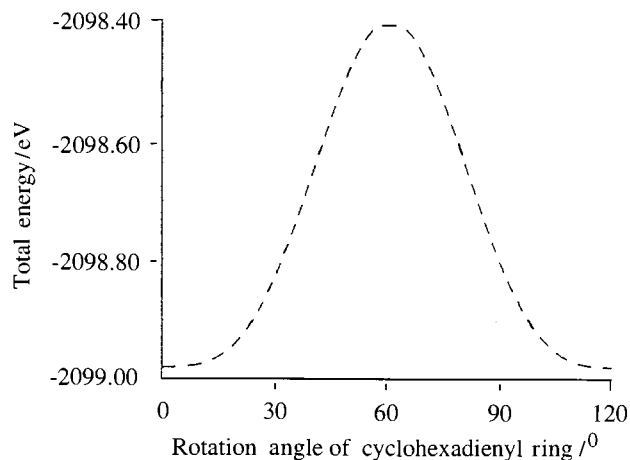


Fig. 9 Variation of the total EHMO energy of **1** as the cyclohexadienyl ring is rotated by 120° in steps of 6°, beginning in an eclipsed conformation.

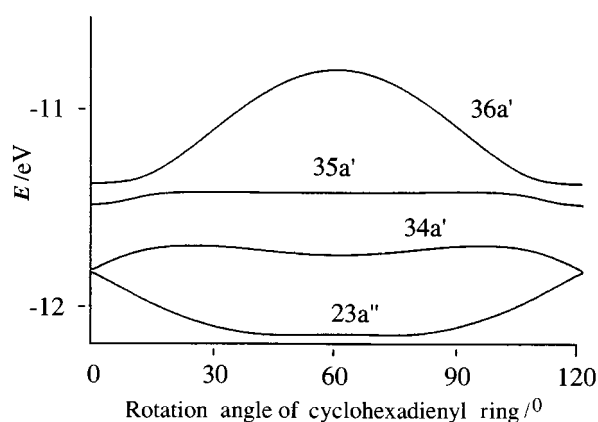


Fig. 10 Variation of the EHMO energies of the 23a''–36a' levels of **1** as the cyclohexadienyl ring is rotated by 120° in steps of 6°, beginning in an eclipsed conformation.

benzene ring in $[\text{Ru}(\eta^6\text{-C}_6\text{H}_6)\{\kappa^3\text{-HB}(\text{Pz})_3\}]^+$, and the resulting energy change is shown in Fig. 9. Clearly the energy change that accompanies rotation of the cyclohexadienyl ring is both qualitatively and quantitatively different from that which occurs during the benzene ring rotation (Fig. 6). In the case of the cyclohexadienyl, 0° of rotation corresponds to the most stable geometry, and the total energy goes through a single maximum at 60°. This maximum energy is 58.1 kJ mol⁻¹ above the most stable orientation, a difference which is significantly greater than in the benzene case. This result supports the experimental evidence from our NMR studies discussed previously.

Before attempting a more detailed explanation of the origin of the much larger rotational barrier in **1**, it is worth noting that the lower symmetry of cyclohexadienyl (C_2) with respect to benzene (D_{6h}) means that there is no infinite axis to rotation in the cyclohexadienyl moiety. Put another way, the interaction of the cyclohexadienyl ring with the metal fragment is much more dependent on the orientation of the ring than is the case in the benzene molecule, resulting in greater energy changes during rotation.

In extended Hückel theory, the total energy of a molecule is given by the sum of the energies of its MOs multiplied by their occupation numbers. Thus the total energy change shown in Fig. 9 is the net effect of the energy changes of the 69 EHMOs of **1**. Clearly we cannot analyse each of these in detail, but we can make progress through the observation that it is the four highest occupied orbitals which experience the greatest changes during rotation of the cyclohexadienyl ring. Indeed the sum of the changes in the energies of the four highest occupied MOs

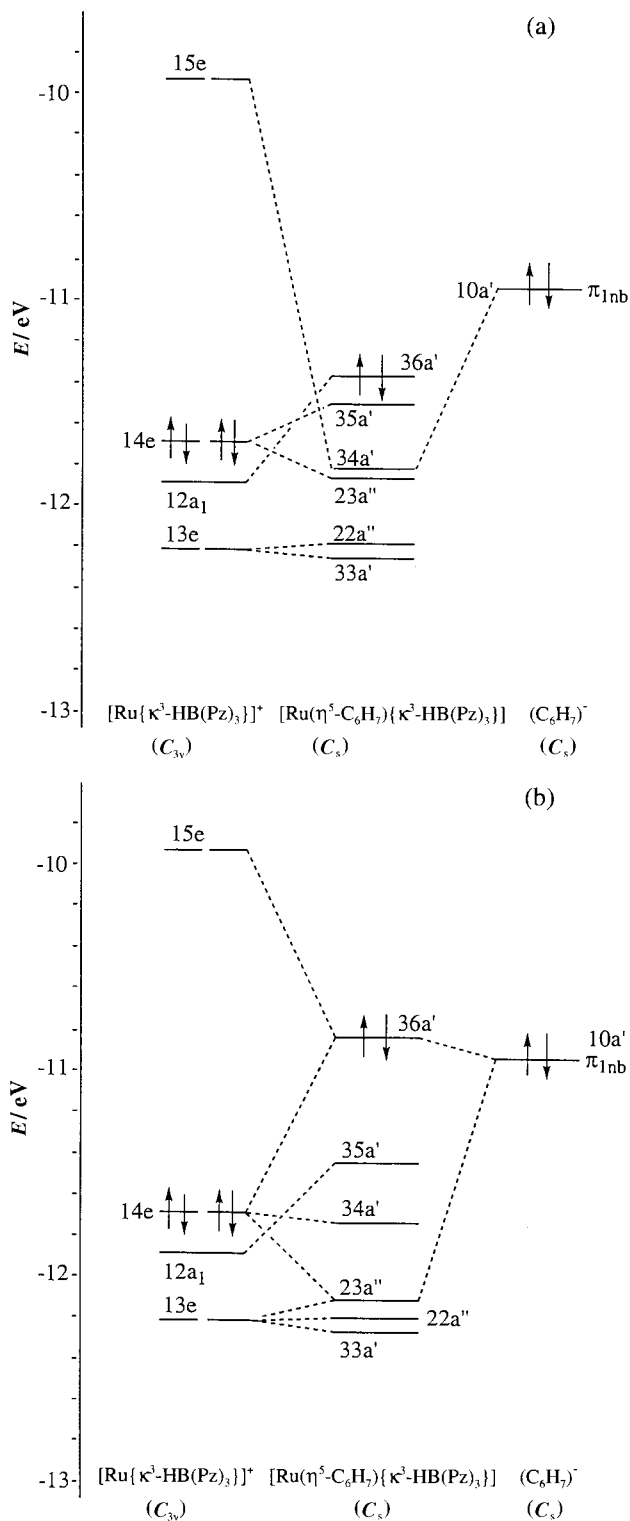


Fig. 11 Fragment EHMO diagram of the highest occupied orbitals of **1** at (a) 0° and (b) 60° of rotation of the cyclohexadienyl ring about the Ru–ring centroid vector.

account for 63% of the rotational barrier, and Fig. 10 plots the energies of the 23a''–36a' levels as the cyclohexadienyl ring is rotated. The 36a' HOMO is most affected by the ring rotation, mirroring the total energy change (Fig. 9). At the starting geometry, this orbital is largely Ru d_{z²}. However, as the ring is rotated the composition of the 36a' MO changes significantly, to the extent that at the least stable geometry (60°) it is a mixture of the 10a' level and the 14e and 15e orbitals of the $[\text{Ru}\{\kappa^3\text{-HB}(\text{Pz})_3\}]^+$ fragment. The destabilisation of the 36a' orbital may therefore be traced to the increasing contribution

of the 15e LUMO of the metal fragment, which is much higher in energy than the Ru d_z^2 orbital.

Fig. 11 presents fragment MO diagrams for the highest occupied MOs of **1** with the cyclohexadienyl ring at 0° (a) and 60° (b) of rotation. As discussed above, the 36a' HOMO is strongly destabilised by the involvement of the 15e [Ru{ κ^3 -HB(Pz)₃}]⁺ fragment LUMO. By contrast, the energy of the 35a' orbital remains largely unaltered as the ring is rotated, although its composition changes significantly. At 0° it is primarily derived from the 14e MO of the metal fragment, but at 60° it has a 90% contribution from the mainly Ru d_z^2 12a₁ [Ru{ κ^3 -HB(Pz)₃}]⁺ fragment level. Thus as the d_z^2 character of the 36a' orbital decreases, that of the 35a' increases. Furthermore, as the 36a' MO gains [Ru{ κ^3 -HB(Pz)₃}]⁺ 15e character, that of the 34a' decreases such that, by 60° of rotation, it is derived largely from the 14e [Ru{ κ^3 -HB(Pz)₃}]⁺ fragment orbital. The 23a'' MO is significantly stabilised upon cyclohexadienyl rotation. At 0°, it has ca. 70% [Ru{ κ^3 -HB(Pz)₃}]⁺ 14e character with only very small contributions from the cyclohexadienyl ligand. At 60°, however, it acquires appreciable cyclohexadienyl 10a' character, as well as having [Ru{ κ^3 -HB(Pz)₃}]⁺ 14e and 13e content. It becomes Ru–cyclohexadienyl bonding upon rotation, which accounts for its energetic stabilisation.

Thus we can see that the rotation of the carbocycle in **1** has a much greater effect upon the valence electronic structure and total energy than in [Ru(η^6 -C₆H₆){ κ^3 -HB(Pz)₃}]⁺. A much larger rotational energy barrier is calculated in **1**, in agreement with experimental data, and that energy barrier is largely explained by the energy and composition variations of the highest occupied MOs. By contrast, the electronic structure of [Ru(η^6 -C₆H₆){ κ^3 -HB(Pz)₃}]⁺ is almost unaffected by ring rotation on account of the high symmetry of the benzene fragment.

Rotation of the cyclohexadienyl ring through 120° about the Ru–cyclohexadienyl centroid vector in **8, **9** and **10**.** Our NMR studies indicate that the magnitude of the rotational barrier in the substituted cyclohexadienyl compounds depends on both the position and size of the substituents. We have therefore attempted to analyse this effect computationally by repeating the ring rotation studies of **1** for **8**, **9** and **10**. Before discussing these results, we must highlight a problem that we encountered upon ring substitution. Replacement of a ring H with, for example, a methyl group produced unrealistically high barriers in systems which are known to have small barriers. For example, replacement of benzene by mesitylene in [Ru(η^6 -C₆H₆){ κ^3 -HB(Pz)₃}]⁺ caused a 12-fold increase in the calculated rotational barrier, which is clearly incompatible with experimental conclusions.²⁵ Similar increases were observed in the substituted cyclohexadienyl rings. In order to establish the origin of these very high barriers we conducted a series of calculations in which the ring substituents in [Ru(η^6 -C₆H₆R){ κ^3 -HB(Pz)₃}]⁺ (R = Me, ⁱPr) were bent out of the plane of the π system and away from the metal fragment. The barriers quickly reduced and returned to sensible values at about 10° of bending. It would appear that the cause of the artificially high barriers is an interaction between the H atoms on the carbocyclic ring substituents and those of the Pz rings of the HB(Pz)₃ ligand which are directed toward the carbocycle. In all our studies of **8**, **9** and **10**, therefore, the Me and ⁱPr substituents are bent by 10° out of the C₅ plane. Clearly this prevents quantitative comparison with our calculated barriers for **1**, but we feel that we are still justified in comparing barriers within the series **8**, **9** and **10**.

The form of the total EHMO energy change of **8** as the cyclohexadienyl ring is rotated by 120° about the Ru–ring centroid axis is very similar to the analogous unsubstituted compound (**1**), with a single maximum at 60° of rotation. The energy barrier (71.8 kJ mol⁻¹) is also quite close to that for **1** but, as we have already discussed, the imposed bending of the methyl groups in **8** precludes any direct comparison with **1**.

Rotation angle of 3,6-diisopropylcyclohexadienyl ring /°

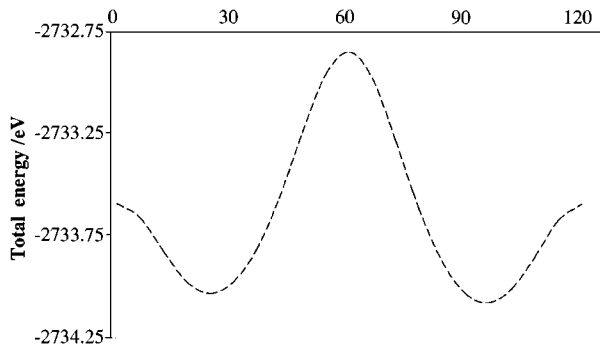


Fig. 12 Variation of the total EHMO energy of **9** as the cyclohexadienyl ring is rotated by 120° in steps of 6°, beginning in an eclipsed conformation.

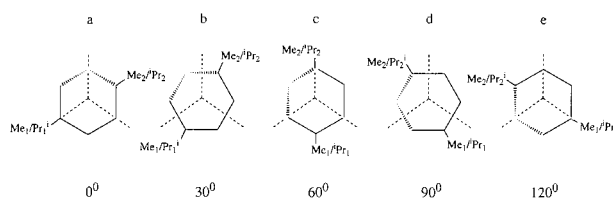


Fig. 13 The conformations adopted by the cyclohexadienyl ring of **8** and **9** at 0°, 30°, 60°, 90° and 120° of rotation about the Ru–ring centroid vector (---- denotes a Pz ring).

The total EHMO variation on 120° rotation of the carbocycle in the bis isopropylated derivative, **9**, is shown in Fig. 12. Clearly this graph is rather different from Fig. 9, with two minima (at 30° and 90°) separated by two maxima (at 0/120° and 60°). The largest energy difference is between 60° and 90° (steps c and d on Fig. 13) and is 118.4 kJ mol⁻¹, 1.65 times greater than the barrier in **8**. Thus the calculated barrier is appreciably greater in the bis isopropylated compound than the bis methylated one, in agreement with the conclusions drawn from our NMR studies.

At this point we must address two questions. The first is why the form of the plots is different for bis isopropylated and bis methylated cyclohexadienyl and the second is why there is a higher rotational barrier in **9** than in **8**. Addressing the second question first, a logical way to proceed is to analyse the variations in the energies of the MOs of **8** and **9** in an analogous manner to our earlier treatment of **1**. Unfortunately this is not a productive approach as the variations are very similar in all three molecules **1**, **8** and **9**, with the combination of the highest occupied orbitals accounting for a substantial part of the barrier in each case. This is unsurprising in that it is well known that substitution of carbocyclic ring H atoms by R groups does not significantly affect the valence electronic structure of the π system, except to produce a general raising (or lowering) of the MO energies.

Given the lack of a clear cut electronic explanation, it is helpful to consider other possible causes of the differences in barrier heights and total energy plots for **8** and **9**, in particular the steric bulk of Me vs. ⁱPr. Fig. 13 suggests that initial rotation of the cyclohexadienyl ring in **8** and **9** might be expected to result in a stabilisation, as Me/ⁱPr₁ moves away from its eclipsed position over one of the Pz rings. There is little or no change in the total energy of **8** for this distortion, although Fig. 12 shows that the analogous rotation for the bis isopropylated ring indeed produces a significant stabilisation. If we assume that the electronic effects are approximately the same for both rings, we may trace the difference in the total energies of **8** and **9** for the first 30° of rotation to the bulk of the R substituent in the 3-position, *i.e.* that the relief of the ⁱPr₁/Pz eclipsing is more energetically favourable than that of the Me₁/Pz.

Between 30° and 60° the total energy of both **8** and **9** becomes significantly less negative (60° is the least stable geometry in both cases). Now both the electronic component and steric component of the barrier are working together, the latter being unfavourable as Me₂/ⁱPr₂ come into an eclipsed geometry with a Pz ring. From 60° to 90° the electronic and steric components again reinforce one another, but this time to stabilise the molecules. The stabilisation is greater for **9** than **8** as the relief of the ⁱPr₂/Pz eclipsing is greater than that of the Me₂/Pz. Finally, from 90° to 120° the eclipsing of Me₁/Pz does not greatly affect the total energy of **8**, in contrast to **9** where the interaction of the bulkier ⁱPr₁ with the Pz ring results in a destabilisation of the molecule.

The variation in the total EHMO energy of **10** as the cyclohexadienyl ring is rotated through 120° is very similar to that of **1** (Fig. 9) and **8**. However, the size of the rotational barrier is calculated to be 156.5 kJ mol⁻¹, 2.18 times greater than that of **8** and 1.32 times that of **9**. This result is again entirely consistent with our NMR experiments, which found that the pyrazolyl signals were sharp at room temperature, implying that **10** has the highest rotational barrier of all the compounds studied. Extension of our previous arguments for **8** and **9** readily explains the high barrier in **10**. If we once again assume that the electronic contribution is similar to that in **1**, then the extra barrier height of **10** arises from the movement of the three methyl groups from staggered→eclipsed→staggered in the course of the 120° rotation.

Conclusions

In this contribution we have described the results of combined experimental and theoretical studies of the cyclohexadienyl compounds that result from nucleophilic attack on [Ru(η⁶-arene){κ³-HB(Pz)₃}]⁺ and [Ru(η⁶-arene){κ³-HC(Pz)₃}]²⁺. Thus, reaction of [Ru(η⁶-arene){κ³-HB(Pz)₃}][PF₆]⁻ with H⁻, CN⁻ or OH⁻ leads to the cyclohexadienyl compounds **1**, **2** and **3**, and the nucleophile has been shown to enter along an *exo* pathway. Similarly, reaction of [Ru(η⁶-arene){κ³-HC(Pz)₃}][PF₆]₂ with CN⁻ forms **11**, which has been characterised crystallographically. Variable temperature NMR experiments indicate that one of the ligands in the cyclohexadienyl compounds undergoes restricted rotation about the metal–ligand axis. This is consistent with the crystal structure of **11**, which reveals that in the solid state the complex cation [Ru(η⁵-C₆H₆CN){κ³-HC(Pz)₃}]⁺ adopts a conformation in which one Pz ring is eclipsed by the projection of the sp³ hybridised C atom of the cyclohexadienyl moiety. Furthermore, variable temperature NMR studies on the cyclohexadienyl compounds that result from the attack of nucleophiles on the substituted arene compounds [Ru(η⁶-arene){κ³-HB(Pz)₃}][PF₆]⁻ (arene = 1-ⁱPr-4-MeC₆H₄, 1,4-Me₂C₆H₄, 1,4-ⁱPr₂C₆H₄ or 1,3,5-Me₃C₆H₃) indicate that the magnitude of the rotational barrier in the cyclohexadienyl compounds is dependent both on the position and number of the substituents on the cyclohexadienyl ring. That it is the cyclohexadienyl ring that is undergoing the restricted rotation is indicated by variable temperature NMR studies of **14** (in which the Pz rings are substituted but the cyclohexadienyl ring is not) which displays a similar coalescence temperature (and therefore a similar rotational barrier) to **1**.

Extended Hückel calculations have been used to investigate the MO structure of [Ru(η⁶-C₆H₆){κ³-HB(Pz)₃}]⁺ and **1** in terms of the [Ru{κ³-HB(Pz)₃}]⁺ and carbocyclic fragments. Subsequent calculations in which the carbocycle was rotated through 120° about the Ru–ring centroid vector revealed a very small energy barrier to rotation in the benzene compound but a significantly greater barrier in the cyclohexadienyl system. This observation is entirely consistent with experiment. The very low barrier in the benzene compound is a consequence of the high symmetry of the benzene ligand, in that the interaction of the ring with the Ru fragment is essentially unaltered as the ring is

rotated. By contrast, the lower symmetry of the cyclohexadienyl ring means that its interaction with the [Ru{κ³-HB(Pz)₃}]⁺ unit is much more dependent upon their relative orientation. More specifically, the greater barrier height in **1** has been analysed in terms of the changes in the composition of the highest occupied MOs during ring rotation. The HOMO is strongly destabilised, on account of the increasing contribution of the high lying LUMO of the [Ru{κ³-HB(Pz)₃}]⁺ fragment.

Calculations on the substituted cyclohexadienyl compounds **8** and **9** also support experiment in finding a greater rotational barrier for the bis isopropylated derivative **9** in comparison with the bis methylated compound **8**. This difference in barrier height is traced to the greater steric bulk of ⁱPr vs. Me, as the electronic effects are found to be very similar in both cases. Finally, the calculated barrier for ring rotation in the tris methylated compound **10** is greater than any of the other systems studied, once again agreeing with the conclusions drawn from our variable temperature NMR data. The cause of this increased barrier height is also attributed to steric effects.

Acknowledgements

We thank Johnson Matthey plc for generous loans of ruthenium trichloride and University College London for financial support (S. B.).

References

- 1 M. R. J. Elsegood, J. W. Steed and D. A. Tocher, *J. Chem. Soc., Dalton Trans.*, 1992, 1797.
- 2 J. W. Steed and D. A. Tocher, *J. Chem. Soc., Dalton Trans.*, 1993, 3187.
- 3 S. G. Davies, M. L. H. Green and D. P. M. Mingos, *Tetrahedron*, 1978, **34**, 3047.
- 4 T. S. Cameron, M. D. Clerk, A. Linden, K. C. Sturge and M. J. Zaworotko, *Organometallics*, 1988, **7**, 2571.
- 5 J. F. Helling and G. G. Cash, *J. Organomet. Chem.*, 1974, **73**, C10.
- 6 D. R. Robertson, I. W. Robertson and T. A. Stephenson, *J. Organomet. Chem.*, 1980, **202**, 309.
- 7 C. C. Neto and D. A. Sweigart, *J. Chem. Soc., Chem. Commun.*, 1990, 1703.
- 8 V. S. Kaganovich, A. R. Kudinov and M. I. Rybinskaya, *J. Organomet. Chem.*, 1987, **323**, 111.
- 9 H. LeBozec, D. Touchard and P. H. Dixneuf, *Adv. Organomet. Chem.*, 1989, **29**, 163.
- 10 S. Bhambri and D. A. Tocher, *Polyhedron*, 1996, **15**, 2763.
- 11 S. Bhambri and D. A. Tocher, *J. Chem. Soc., Dalton Trans.*, 1997, 3367.
- 12 S. Bhambri and D. A. Tocher, *J. Organomet. Chem.*, 1996, **507**, 291.
- 13 G. M. Sheldrick, SHELXS-86, *Acta Crystallogr., Sect. A*, 1990, **46**, 467.
- 14 G. M. Sheldrick, SHELXL-93, University of Göttingen, 1993.
- 15 C. Mealli and D. M. Proserpio, *J. Chem. Educ.*, 1990, **67**, 399.
- 16 R. Hoffmann and W. N. Lipscomb, *J. Chem. Phys.*, 1962, **36**, 2179.
- 17 R. Hoffmann, *J. Chem. Phys.*, 1963, **39**, 1397.
- 18 R. S. Mulliken, *J. Chem. Phys.*, 1955, **23**, 1833, 1841, 2338, 2343.
- 19 Z. Shirin, R. Mukherjee, J. F. Richardson and R. M. Buchanan, *J. Chem. Soc., Dalton Trans.*, 1994, 465.
- 20 R. T. Swann, A. W. Hanson and V. Boekelheide, *J. Am. Chem. Soc.*, 1986, **108**, 3324.
- 21 G. Winkhaus, L. Pratt and G. Wilkinson, *J. Chem. Soc.*, 1961, 3807.
- 22 M. Keys, V. G. Young and W. B. Tolman, *Organometallics*, 1996, **15**, 4133.
- 23 W. D. Jones and E. T. Hessel, *Inorg. Chem.*, 1991, **30**, 781.
- 24 F. A. Cotton, *Chemical Applications of Group Theory*, Wiley-Interscience, New York, 3rd edn., 1991.
- 25 D. Braga, *Chem. Rev.*, 1992, **92**, 633.
- 26 T. A. Albright, P. Hofman and R. Hoffmann, *J. Am. Chem. Soc.*, 1977, **99**, 7546.
- 27 D. O'Hare, S. J. Heyes, S. Barlow and S. Mason, *J. Chem. Soc., Dalton Trans.*, 1996, 2989.
- 28 K. D. Warren, *Struct. Bonding (Berlin)*, 1976, **27**, 45.
- 29 J. G. Brennan, G. Cooper, J. C. Green, N. Kaltsoyannis, M. A. MacDonald, M. P. Payne, C. M. Redfern and K. H. Sze, *Chem. Phys.*, 1992, **164**, 271.
- 30 J. C. Green, N. Kaltsoyannis, M. A. MacDonald and K. H. Sze, *J. Am. Chem. Soc.*, 1994, **116**, 1994.